ANNALS OF GEOPHYSICS, 69, 2, 2026; doi:10.4401/ag-9487
OPEN ACCESS

Unraveling the Rupture Properties of Four Destructive Earthquakes in Türkiye (1966-1975)

Murat Utkucu[1,2], Şeyma Berzah[1,2], Fatih Uzunca[2,3], Hatice Durmuş[*,4], Süleyman Sami Nalbant[5]

(1) Sakarya University, Engineering Faculty, Department of Geophysics, Sakarya, Türkiye
(2) Sakarya University, Institute of Natural Sciences, Sakarya, Türkiye
(3) The Ministry of Environment, Urbanization and Climate Change, Urban Transformation Presidency, Sakarya, Türkiye
(4) Kütahya Dumlupınar University, Engineering Faculty, Department of Geological Engineering, Kütahya, Türkiye
(5) Iğdır University, Faculty of Science and Literature, Geography Department, Iğdır, Türkiye

Article history: received November 3, 2025; accepted March 17, 2026

Abstract

This study presents finite-fault rupture models for four destructive earthquakes in Türkiye: the 1966 Varto ($M_W = 6.7$), 1967 Mudurnu Valley ($M_W = 7.3$), 1971 Bingöl ($M_W = 6.7$), and 1975 Lice ($M_W = 6.6$) events. Using a teleseismic waveform inversion technique, we derive the spatial distribution of slip, rupture geometry, and seismic moment for each earthquake. Our models reveal that the ruptures are characterized by distinct asperities and are significantly influenced by geometric fault complexities such as bends and step-overs. The 1966 Varto earthquake involved oblique faulting with three asperities. The 1967 Mudurnu Valley rupture is dominated by a large asperity, with propagation affected by a 20-degree fault bend. The 1971 Bingöl earthquake model supports the segmentation of the East Anatolian Fault Zone at the Göynük Bend and suggests further sub-segmentation of the Ilıca Fault Segment at a geometric discontinuity corresponding to the northeastern edge of a large asperity. The 1975 Lice earthquake model shows rupture arrest at a western fault step-over. These results underscore the critical role of structural discontinuities in controlling rupture initiation, propagation, and termination, providing essential insights for seismic hazard assessment in these tectonically active regions.

Keywords: 1966 Varto earthquake; 1967 Mudurnu Valley earthquake; 1971 Bingöl earthquake; 1975 Lice earthquake; Teleseismic Finite-fault inversion

1. Introduction

Understanding the rupture characteristics of an earthquake is fundamental to understanding its preparation and coseismic phases. Finite-fault rupture models, which provide the spatial distribution of slip over the causative faults, are crucial for defining fault segments, identifying seismic gaps, and locating areas of creep or locking at depth (Oppenheimer et al., 1990; Wald et al., 1991; Sieh, 1996). These models also provide valuable information for constructing earthquake recurrence models.

Strong ground motion records from large, damaging earthquakes are valuable for engineering applications. However, many major historical earthquakes were either not recorded or lacked a sufficient number of strong-motion records. Consequently, the need to compute near-field records for such events has led to the development of numerous computational methods (Hall et al., 1995; Beresnev and Atkinson, 1998; Boore, 2009). This effort has resulted in the expansion of strong motion databases and the improvement of building codes. It has been demonstrated that finite-fault characteristics such as rupture length and width, the number and size of asperities, and displacement rise-time significantly affect strong ground motion recordings, particularly at close distances (Graves, 1998). This makes finite-fault source models essential for synthetically generating strong ground motion records in earthquake-prone areas (Hall et al., 1995; Beresnev and Atkinson, 1997; Somerville et al., 1997).

In the present study, finite-fault rupture models for four destructive earthquakes occurred in Türkiye are obtained using a teleseismic waveform inversion technique developed by Kikuchi et al. (2003). These earthquakes are the 19 August 1966 Varto ($M_W = 6.7$), the 22 July 1967 Mudurnu Valley ($M_W = 7.3$), the 22 May 1971 Bingöl ($M_W = 6.7$), and the 6 September 1975 Lice ($M_W = 6.6$) earthquakes (Fig. 1). All these earthquakes occurred in different tectonic domains before the digital recording era. They are important because their ruptures are either on or in the close vicinity of the North Anatolian Fault Zone (NAFZ) and the East Anatolian Fault Zone (EAFZ), which are the major sources of the earthquake hazard in Türkiye. Therefore, further information to constrain their ruptures from the digitized analog records would be valuable for understanding the earthquake interaction, rupture behavior and seismic hazard of these major fault zones.

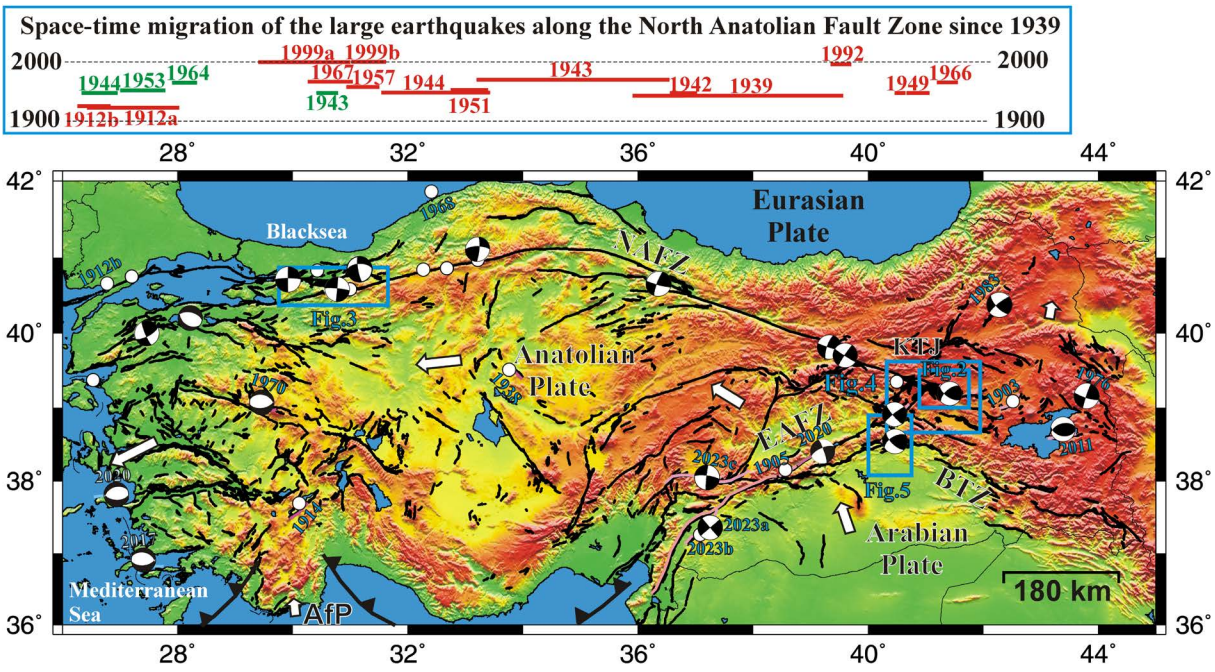

Figure 1. Map showing major tectonic elements of Türkiye along with the earthquake epicentres (white circles), focal mechanisms (centred at the respective earthquakes' epicentres) and rupture extents of the $M_W \geq 6.5$ earthquakes in the instrumental period. The red lines in the top panel represent the earthquake ruptures along the main and the Northern Strand of the North Anatolian Fault Zone (NAFZ), while the green lines indicate ruptures along the other strands. The other earthquake ruptures are shown with pink lines on the map. Blue rectangles enclose the map areas shown in Figs. 2-5. Large arrows represent the direction of relative plate motions with respect to the stable Eurasian Plate. Note the westward space-time migration of the earthquakes between 1939 and 1999 along the NAFZ. Compiled from Barka and Kadinsky-Cade (1988), Barka (1996), Şengör et al. (2005), Reilinger et al. (2006), Tan et al. (2008), Emre et al. (2013) and references therein. AfP: African Plate, EAFZ: East Anatolian Fault Zone, KTJ: Karlıova Triple Junction, BTZ: Bitlis Thrust Zone.

2. Seismotectonics

The active tectonics of Türkiye and its surrounding regions are primarily controlled by the northward convergence of the Arabian and African plates relative to the Eurasian plate (Fig. 1) (McClusky et al., 2000; Reilinger et al., 2006; England et al., 2016). As a result, the Anatolian Plate moves westward along two major strike-slip fault systems: The NAFZ and the EAFZ (Arpat and Şaroğlu, 1972; Barka and Kadinsky-Cade, 1988; Şaroğlu et al., 1992; Şengör et al., 2005; Emre et al., 2013; Duman and Emre, 2013). The NAFZ and EAFZ intersect at the Karlıova Triple Junction (KTJ) in eastern Türkiye. The westward motion of the Anatolian Plate turns towards the southwest in western Türkiye, creating an extensional tectonic regime (Taymaz et al., 1991a; Nyst and Thatcher, 2004; Aktuğ et al., 2009; Jolivet et al., 2013). The African Plate subducts beneath the Anatolian Plate along the Cretan and Cyprus arcs (Wdowinski et al., 2006; Shaw and Jackson, 2010), while the Bitlis Thrust Zone (BTZ) marks the boundary between the Arabian Plate and the Eastern Anatolian Block (Eyidoğan, 1983; Copley and Jackson, 2006; Seyitoğlu et al., 2017). This tectonic framework has been confirmed by GPS (Global Positioning System) measurements (Reilinger et al., 2006; Vernant, 2015; Özbakır et al., 2017; England et al., 2016). The GPS studies also suggest that the Anatolian Plate behaves relatively rigidly, hosting only one $M_W \geq 6.5$ earthquake, the 1938 Kırşehir earthquake, in the instrumental period (Ambraseys 1988, 2001). At this point, the occurrence of the 1968 Bartın earthquake with a dominant reverse faulting mechanism along the Black Sea coast should also be mentioned by means of diffuse deformation around the NAFZ (Alptekin et al., 1986).

The main strand of the NAFZ produced 12 large ($M_W \geq 6.5$), devastating and surface-rupturing earthquakes, including the 1967 Mudurnu Valley earthquake and 1999 İzmit and Düzce earthquake doublet in the 20th century (Barka 1996, Şengör et al., 2005) (Fig. 1). Nine of these earthquakes migrated westward along the fault in both time and space. The migration has been well explained by the earthquake stress interactions (Stein et al., 1997; Lorenzo-Martin et al., 2006). The 1944, 1953 and 1964 earthquakes occurred along the Southern Strand of the NAFZ in NW Türkiye. All of these NAFZ earthquakes were due to dominant strike-slip faulting, excluding the 1944 Edremit (along the Aegean coast) and the 1964 Manyas earthquakes with dominant normal faulting, reflecting locally developed extensions between the fault segments of the NAFZ (Fig. 1) (Şengör et al., 2005; Tan et al., 2008). On the contrary, the EAFZ was relatively quiet in the 20th century, compared to the 19th century (Ambraseys 1989). The 1905 Malatya and 1971 Bingöl earthquakes were the only $M_W \geq 6.5$ earthquakes to occur along the EAFZ in the 20th century (Ambraseys 1989; Duman and Emre 2013). Nevertheless, the 2020 Sivrice-Doğanyol and 2023 Pazarcık-Elbistan earthquake doublet and a following $M_W = 6.7$ aftershock imply that the 21st century will be a highly active period.

Some studies discussed that the NAFZ extends in the eastern Anatolian block in the east of the KTJ and merges with the main right lateral faults related to the Zagros Thrust Belt in Iran (Ketin, 1977; Jackson 1992), taking into account occurrence of the 1966 Varto and 1976 Çaldıran earthquakes in Türkiye, and 1930 Salmas earthquake in Iran (Stewart and Kanamori 1982; Toksöz et al., 1978; Ambraseys 1988, 2001; Ambraseys and Jackson 1998). The deformation caused by the Arabian Plate convergence along the BTZ is mostly transferred to the eastern Anatolian block (McClusky et al., 2000; Reilinger et al., 2006). This deformation is largely conveyed to the Caucasus thrust zones through the distributed NW-SE trending dextral and NE-SW trending sinistral faults, NW-SE trending dextral faults within the eastern Anatolia (Barka and Cadinsky-Cade, 1988; McClusky et al., 2000; Koçyiğit et al., 2001; Reilinger et al., 2006). The 1975 Lice earthquake is the only instrumental period $M_W \geq 6.5$ earthquake to take place along the BTZ with oblique faulting (Taymaz et al., 1991b; Tan et al., 2008). Nevertheless, there are 3 $M_W \geq 6.5$ strike-slip earthquakes (1903, Malazgirt, 1976 Çaldıran and 1983 Horasan-Narman earthquakes) within eastern Anatolia (Stewart and Kanamori 1982; Toksöz et al., 1977; Ambraseys and Jackson 1998, Eyidoğan et al., 1999; Ambraseys 2001). The 2011 Van earthquake with dominant reverse faulting also evidences the presence of compression (Utkucu, 2013).

In western Anatolia, the instrumental period $M_W \geq 6.5$ earthquakes with known source mechanisms are the 1970 Gediz, 2017 Bodrum and 2020 İzmir-Samos earthquakes, all of which have virtually pure normal faulting mechanisms requiring roughly N-S extension (Eyidoğan and Jakson 1985; Karasözen et al., 2018; Kiratzi et al., 2021). Overall, all of the available source mechanisms of the instrumental period $M_W \geq 6.5$ earthquakes are in good agreement with the regional plate kinematics derived from the GPS data (Reilinger et al., 2006; Vernant, 2015; Özbakır et al., 2017; England et al., 2016).

3. Teleseismic Data

In this study, digitized teleseismic P-waveforms from World Wide Standardized Seismograph Network (WWSSN) analog records were used for the finite-fault inversions (Pınar, 1995). After correcting for instrument responses, the arrival times of the P-wave phases at each station were determined based on the earthquakes' epicentral locations using the travel-time tables of Jeffreys and Bullen (1958). After a visual inspection, minor adjustments were made to arrival times at some stations where necessary. To eliminate long-period oscillations and high-frequency noise, the data were band-pass filtered from 0.05 to 1 Hz. The data were digitized at sampling intervals of 0.5 and 1.0 s for the 1967 Mudurnu Valley and the other earthquakes, respectively. The number of stations and time window lengths used in the inversions are as follows: 18-40 s for the 1966 Varto earthquake, 19-45 s for the 1967 Mudurnu Valley earthquake, 21-50 s for the 1971 Bingöl earthquake, and 16-35 s for the 1975 Lice earthquake (Fig. S1).

4. Method

The Finite-Fault Inversion Method developed by Kikuchi et al. (2003) was used to model the long-period P-waveforms. The framework of this method is similar to the finite-fault inversion approach presented by Hartzell and Heaton (1983). To obtain the spatial distribution of slip, the earthquake rupture plane is approximated by a prescribed grid of point sources with fixed strike, dip, and dimensions. The point sources were distributed at equal intervals along the strike and dip directions, with strike and dip angles determined from previous seismological and geological studies. The hypocenter location is identified on the grid, which is embedded in the crustal velocity structure of the source region. A maximum rupture velocity and source time function are then defined for calculating Green's functions (synthetic seismograms).

The rupture velocity of an earthquake generally changes in the range 80-90 per cent of the local shear wave velocity (Mendoza and Hartzell 1988). Hartzell et al. (1991) pointed out that the overall source characteristic of an earthquake is well preserved for rupture velocities ranging 2.1-3.1. In the present study, initial maximum rupture velocities are taken as 3.0 km/s, which corresponds to 80-90 per cent of the shear velocities in the upper crustal depth in the velocity structure used (Table 1). Nevertheless, several inversion trials with different maximum rupture velocities are implemented to find a value that explains the data better for each of the studied earthquakes (Tables S1-S4). Additionally, some flexibility in the rupture velocities is also achieved by introducing time windows parameterization, which permits locally slower rupture velocities than initially assigned values for accommodating rupture complexities (Hartzell and Heaton, 1983; Wald and Heaton, 1994, Kikuchi et al., 2003).

Let $G_{gkj}(t)$ be the Green's function generated by slip in the k-th direction (k = 1, 2) for a unit moment and an isosceles triangular source time function of width 2τ (with rise and fall of τ) at the j-th station (Kikuchi et al., 2003). When the source time function is represented by Nh isosceles triangular functions, each delayed by time τ from the previous one, the synthetic seismogram is given by:

$$y_j(t) = \sum_g \sum_h \sum_k D_{ghk} G_{gkj}\left(t - t_g - (h-1)_\tau\right) \tag{1}$$

Here, D_{ghk} represents the unknown model parameters, and t_g denotes the starting time of fault slip at the g-th node. The synthetic seismograms were calculated using the Reflectivity Method (Koketsu, 1985) and the crustal velocity structure provided by Kenar and Toksöz (1989) (Table 1). The D_{ghk} values are computed using the Least Squares (LS) method. The error of the calculation is expressed as:

$$\Delta = \sum_j \int w_j \left\{x_j(t) - y_j(t)\right\}^2 dt = minimum \tag{2}$$

Here, $x_j(t)$ denotes the j-th observed data, and w_j (>0) represents the relative weighting factor for the j-th record. One constraint is a limited range of variation for the initially defined rake angle. It is assumed that the rake angle of the slip vector varies within ±45° of an initial (λ_0). The slip vector is decomposed into two components with

rake angles of $\lambda_0 + 45^o$ and $\lambda_0 - 45^o$ and the solution is constrained to be non-negative. Another constraint is the smoothing of the spatial slip distribution (Yoshida, 1995; Yagi et al., 1999).

Table 1. Crustal velocity structure used in the waveform inversion of the studied earthquakes (modified from Kenar and Toksöz (1989)).

Thickness (km)	V_P (km/s)	V_S (km/s)	ρ (kg/m^3)
5	4.60	3.00	2660
16	5.80	3.29	2750
20	7.00	3.89	2880
—	8.10	4.44	3300

5. Studied Earthquakes

5.1 The 19 August 1966 Varto earthquake

Studies east of the KTJ indicate the presence of numerous fault segments parallel to the NAFZ's extension (Fig. 2) (Emre et al., 2013; Gürboğa, 2015; Karaoğlu et al., 2017). These faults resemble "horsetail" structures at the termination

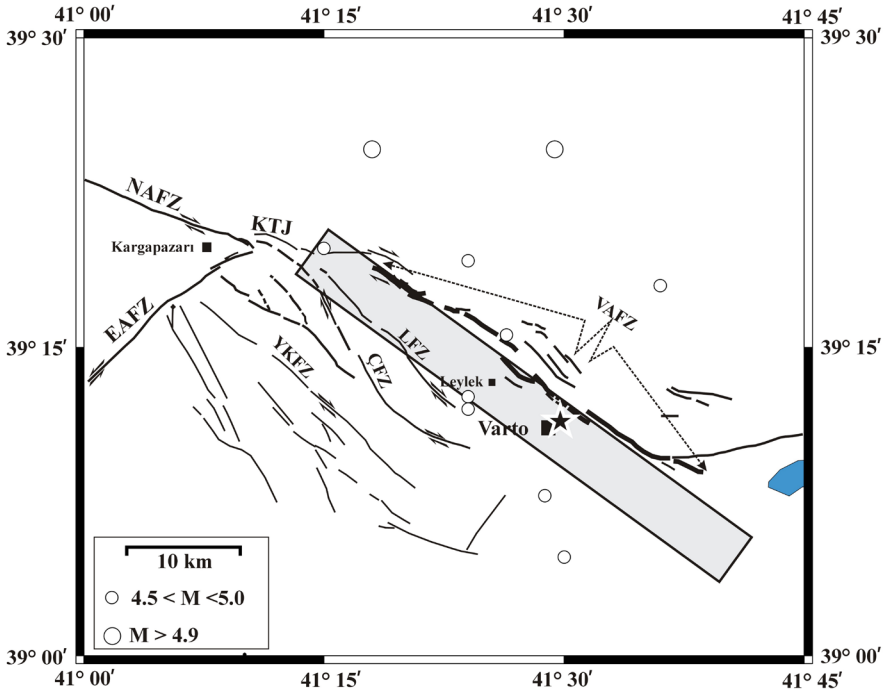

Figure 2. Location map showing the epicenter of the 19 August 1966 Varto earthquake (black star), aftershocks listed in the earthquake catalogs (white circles), the faults extending in the source region (Emre et al., 2013; Karaoğlu et al., 2016), and the surface projection of the model fault plane defined to represent the 1966 earthquake in the present study (grey shaded rectangle). Surface ruptures observed in the field are indicated by thick black lines (Wallace, 1968; Emre et al., 2013). NAFZ: North Anatolian Fault Zone; EAFZ: East Anatolian Fault Zone; KTJ: Karlıova Triple Junction; VAFZ: Varto Fault Zone; ÇFZ: Çayçatı Fault Zone; LFZ: Leylek Fault Zone; YKFZ: Yorgan Çayır-Kaynarca Fault Zone.

of strike-slip faults (Kim and Sanderson, 2006; Kirkpatrick et al., 2008). The Varto Fault Zone (VAFZ), Çayçatı Fault Zone, Leylek Fault Zone, and Yorgan Çayır-Kaynarca Fault Zone are among these structures (Fig. 2). The 1966 Varto earthquake occurred on the northernmost segment, the VAFZ. Geological cross-sections by Karaoğlu et al. (2017) show the fault dipping to the northeast, whereas Gürboğa (2015) suggests a dip to the southwest.

The 1966 Varto earthquake and its significant aftershock sequence, including an $M_S = 6.0$ event (Fig. 2), destroyed more than 19,000 buildings, killed approximately 2,500 people, injured 1,300, and left nearly 100,000 homeless (Ambraseys and Zatopek, 1967, 1968; Wallace, 1968; Berzah, 2018). Field observations revealed discontinuous, predominantly right-lateral strike-slip surface ruptures trending NW-SE (Ambraseys and Zatopek, 1967, 1968; Wallace, 1968). Based on these observations, it was proposed that the earthquake occurred along a possible eastern extension of the NAFZ (Wallace, 1968). Focal and source parameters from various studies are listed in Table 2 (Nowroozi, 1972; Dewey, 1976; Stewart and Kanamori, 1982; Jackson and McKenzie, 1984; Pınar, 1995).

5.2 The 22 July 1967 Mudurnu Valley earthquake

Before the 1999 İzmit earthquake, the 1967 Mudurnu Valley event represented the final event in the westward migration of large earthquakes that started with the 1939 Erzincan earthquake along the NAFZ (Figs. 1 and 3a) (Barka, 1996; Stein et al., 1997). The earthquake caused 86 fatalities, 332 injuries, and the destruction of over 5,000 structures (Ambraseys and Zatopek, 1969; Uzsoy and Ersoy, 1969). An 80-km-long surface rupture was reported, with maximum displacements of 180 cm right-lateral and 120 cm vertical (Figs. 3a and b) (Ambraseys and Zatopek, 1969; Barka, 1996; Muller et al., 2003).

Based on the amplitude spectra of G2 and G3 waves, Canıtez (1972) estimated a rupture length of 80 km, with approximately 55 km propagating westward (Table 2). Given the hypocenter's location near the eastern end of the surface rupture, the rupture is inferred to have propagated unilaterally to the west (Fig. 3a). Focal mechanism solutions indicate pure right-lateral strike-slip faulting and a complex, multi-shock rupture process (Stewart and Kanamori, 1982; Taymaz et al., 1991a; Pınar et al., 1996). The focal and source parameters are compiled in Table 2.

Table 2. Source parameters of the studied earthquakes were obtained from previous studies.

19 August 1966 Varto Earthquake					
	Dewey (1976)	Nowroozi (1972)[a]	Stewart and Kanamori (1982)[a]	Pınar (1995)[b]	
Strike (°)		285	298	110	
Dip (°)		75	65	72	
Rake Angle (°)		−170	145	148	
M_o ($\times 10^{18}$Nm)				9.4	
Stress Shadow (Mpa)				2.5	
Latitude (°)	39.19				
Longitude (°)	41.48				
Depth (km)				6*	
Origin Time	12:22:10				

[a] Fault-plane solution from P-wave first motions; [b] From the inversion of teleseismic long-period P waves; [c] From the inversion of teleseismic P and SH waves; [d] From the amplitude spectrum of G2 and G3 waves; * Source depth; ** Centroid coordinate; *** Centroid depth. KOERI: Kandilli Observatory and Earthquake Research Institute.

22 July 1967 Mudurnu Valley Earthquake					
	Dewey (1976)	Stewart and Kanamori (1982)[a, b]	Taymaz et al. (1991)[c]	Pınar (1995)[b]	Canıtez (1972)[a, d]
		[a]/[b]		Shock1/Total	
Strike (°)		273/	275	276/280	278
Dip (°)		88/	88	90/90	88
Rake Angle (°)			−178	−180/−179	
M_o (10^{18}Nm)		/150	75	44.5/110	
Rupture Length (km)					80
Stress Shadow (MPa)				4.2/	
Latitude (°)	40.57				40.60
Longitude (°)	30.80				31.05
22 May 1971 Bingöl Earthquake					
	Dewey (1976)	Jackson and McKenzie (1984)[a]	Taymaz et al. (1991)[c]	Pınar (1995)[b]	Utkucu et al. (2003)[b]
			Shock1/Shock2	Shock1/Total	
Strike (°)		52/143	231/232	234/226	
Dip (°)		86/82	82/71	84/86	
Rake Angle (°)			3 ± 10/16	4/12	
M_o ($\times 10^{18}$ Nm)			5.8/3.5	9.5/17.50	11
Stress Shadow (MPa)				4.3	
Latitude (°)	38.87	38.83	40.52/40.42**		
Longitude (°)	40.48	40.52	38.89/38.85**		
Depth (km)		3	9 ± /6***	9	
Slip (m)					0.7

[a] Fault-plane solution from P-wave first motions; [b] From the inversion of teleseismic long-period P waves; [c] From the inversion of teleseismic P and SH waves; [d] From the amplitude spectrum of G2 and G3 waves; * Source depth; ** Centroid coordinate; *** Centroid depth. KOERI: Kandilli Observatory and Earthquake Research Institute.

6 September 1975 Lice Earthquake					
	KOERI	Jackson and McKenzie (1984)[a]	Eyidoğan (1980, 1983)	Pınar (1995)[b]	
				Shock1/ Shock2/Total	
Strike (°)		244	254-250	307/231/242	
Dip (°)		54	54-54	66/57/58	
Rake Angle (°)		40	40-40	64/12/27	
M_o ($\times 10^{18}$ Nm)				2.2/6.8/6.21	
Stress Shadow (Mpa)			48-88	1.0/1.8	
Latitude (°)	38.57				
Longitude (°)	40.77				
Depth (km)	26			5/11/*	
Origin Time	09:20:12				

[a] Fault-plane solution from P-wave first motions; [b] From the inversion of teleseismic long-period P waves; [c] From the inversion of teleseismic P and SH waves; [d] From the amplitude spectrum of G2 and G3 waves; * Source depth; ** Centroid coordinate; *** Centroid depth. KOERI: Kandilli Observatory and Earthquake Research Institute.

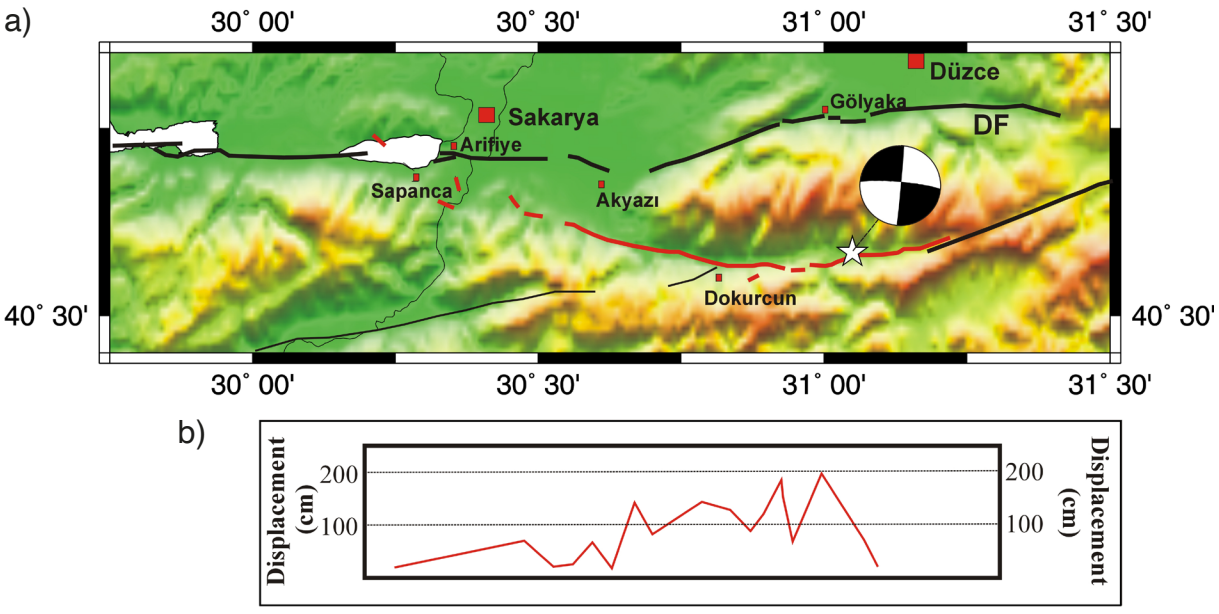

Figure 3. (a) Mapped surface ruptures (red lines) and (b) measured surface displacements of the 1967 Mudurnu Valley earthquake (Ambraseys and Zatopek, 1969; Barka 1996). White star shows the epicenter given by Canıtez 1972 (see Table 2). DF = Düzce Fault.

5.3 The 22 May 1971 Bingöl earthquake

The 1971 Bingöl earthquake ($M_S = 6.7$) occurred along the Ilıca Fault Segment (IFS) of the Karlıova-Ilıca Fault Segment (KIFS), which forms the northernmost part of the EAFZ (Figs. 1 and 4) (Arpat and Şaroğlu, 1972; Seymen and Aydın, 1972; Barka and Kadinsky-Cade, 1988; Şaroğlu et al., 1992; Duman and Emre, 2013). The earthquake caused significant damage in Bingöl city and surrounding settlements, resulting in 755 fatalities (Arpat and Şaroğlu, 1972; Seymen and Aydın, 1972; Eyidoğan et al., 1991). The KIFS extends roughly N50°E between Bingöl city center in the south and the KTJ near Karlıova town in the north (Fig. 4) (Arpat and Şaroğlu, 1972; Seymen and Aydın, 1972; Şaroğlu et al., 1992; Duman and Emre, 2013). Although the IFS disappears beneath the Bingöl Plain, it becomes prominent in the Göynük Valley and can be traced as a single strand for about 13 km toward the NE. It continues for an additional 38 km as the Karlıova Segment (KS) until reaching the KTJ.

Table 3. The earthquakes with magnitude *M*s ≥ 6.0 occurred in the vicinity of the KTJ after the 1866 Göynük earthquake.

No.	Date	Lat-Lon (°)	Origin Time	Name	M_S	M_W	Reference
1	12.05.1866	39.20-41.00		Gönek	7.0-7.2		A1,AJ
2	17.08.1949	39.40-40.65		Kığı	6.7		MK, DW
3	19.08.1966	39.19-41.48		Varto	6.9		DW, MK, AZ
4	20.08.1966	39.37-40.89	11.59.09.0		6.3		DW, A2
5	20.08.1966	39.06-40.76	12.01.43.7	Göynük	6.3		DW, A2
6	26.07.1967	39.49-40.31		Kığı	6.1		DW, MK, A2, AJ
7	22.05.1971	38.83-40.52		Bingöl	6.8		DW, A2, JM
8	01.05.2003	39.01-40.46		Bingöl	6.4	6.4	KOERI, USGS

A1 = Ambraseys (1997); AJ = Ambraseys and Jackson (1998); MK = McKenzie (1972); DW = Dewey (1976); AZ = Ambraseys and Zatopek (1968); A2 = Ambraseys (2001); JM = Jackson and McKenzie (1984); KOERI = Kandilli Observatory and Earthquake Research Institute; USGS = United States Geological Survey.

The 1971 earthquake produced left-lateral surface ruptures along the IFS, extending discontinuously for ~35 km in an en-echelon geometry with a general strike of N40°-45°E (Fig. 4) (Arpat and Şaroğlu, 1972; Seymen and Aydın, 1972; Şaroğlu et al., 1992). Left-lateral slips of up to 0.25 m were measured. Focal mechanisms and waveform modeling indicate left-lateral strike-slip faulting (Table 2; Fig. 4) (Jackson and McKenzie, 1984; Taymaz et al., 1991b; Pınar, 1995). The NE-SW striking nodal plane is consistent with the EAFZ orientation and is interpreted as the fault plane. The 1971 Bingöl earthquake is the first major 20th-century event on the EAFZ for which instrumental epicenter coordinates, surface ruptures, and source mechanism solutions are available (Table 3; Fig. 4).

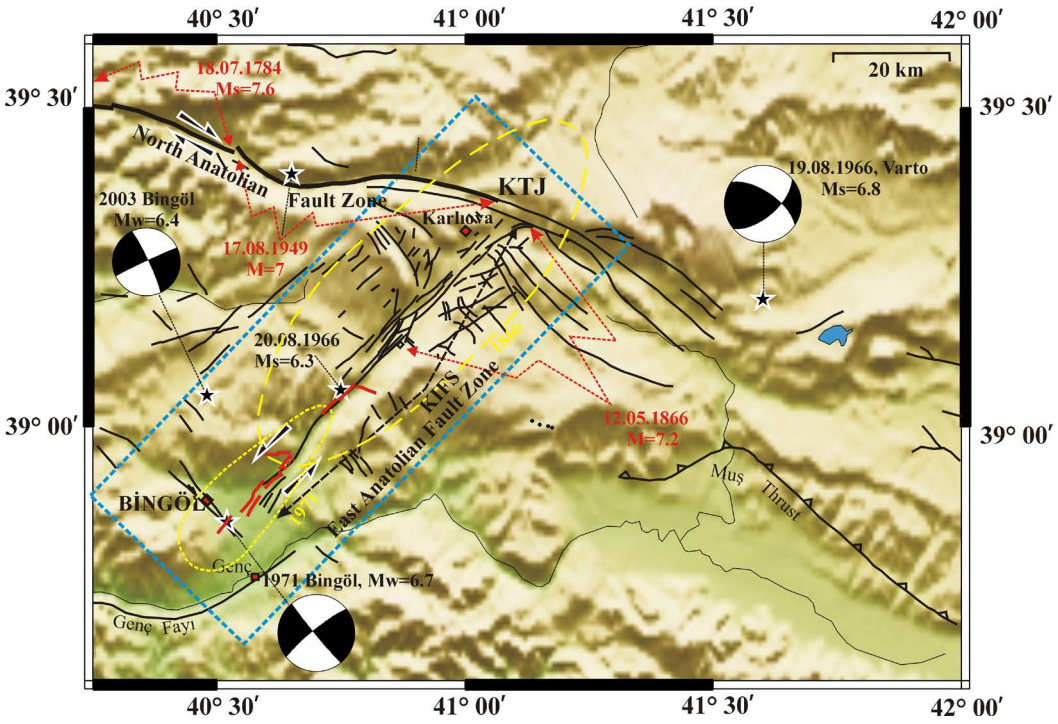

Figure 4. Location map showing the seismotectonic features of the Karlıova Triple Junction (KTJ) region. The yellow dashed/broken lines delineate areas affected by the 1866 Göynük and 1971 Bingöl earthquakes, where reported intensities vary between VIII and IX. The blue rectangle outlines the map area shown in Figs. 11a and 15b. Red continuous lines indicate mapped surface ruptures of the 1971 Bingöl earthquake. See Table 2 and 3 for the earthquake parameters. The data are compiled from Şaroğlu et al. (1992), Seymen and Aydın (1972), Dewey (1976), Barka and Kadinsky-Cade (1988), Ambraseys (1997), Taymaz et al. (1991b), and Pınar (1995). Stars denote the epicentres of the labelled earthquakes. KIFS: Karlıova Ilıca Fault Segment.

5.4 The 6 September 1975 Lice earthquake

The 1975 Lice earthquake occurred along the Bitlis Thrust Zone (BTZ), approximately 50 km south of the EAFZ (Figs. 1 and 5) (Arpat, 1977; Eyidoğan, 1983; Taymaz et al., 1991b; Pınar, 1995). The earthquake caused 2,384 fatalities and the collapse or severe damage of 8,149 buildings (Arpat, 1977). The town of Lice and nearby villages (Kumluca, Yaprak, Yünlüce, Yeşilburç, Gürbeyli, Yamaçlı) suffered heavy damage (Fig. 5) (Arpat, 1977).

The earthquake was generated by the Lice Fault (LF) within the BTZ (Figs. 1 and 5) (Arpat, 1977). Petroleum drilling data indicate the northwestern block of the fault is downthrown by 500-900 m (Perinçek et al., 1987; İmamoğlu and Çetin, 2007). Left-lateral displacement was also identified. Source parameters confirm oblique slip (Table 2; Fig. 5) (Eyidoğan, 1980, 1983; Jackson and McKenzie, 1984; Taymaz et al., 1991b; Pınar, 1995; Berzah, 2018), indicating rupture on a NE-SW striking plane dipping to the NW. Pınar (1995) proposed a two-sub-event rupture process.

Discontinuous surface ruptures and localized uplifts were observed along a length of ~40 km (Fig. 5) (Arpat, 1977). The ruptures indicate roughly N-S oriented compressional deformation between Tuzla and Yaprak villages. Vertical uplifts of ~60 cm were observed southeast of Dernek, and left-lateral displacements of ~13-14 cm were measured east of Yamaçlı village.

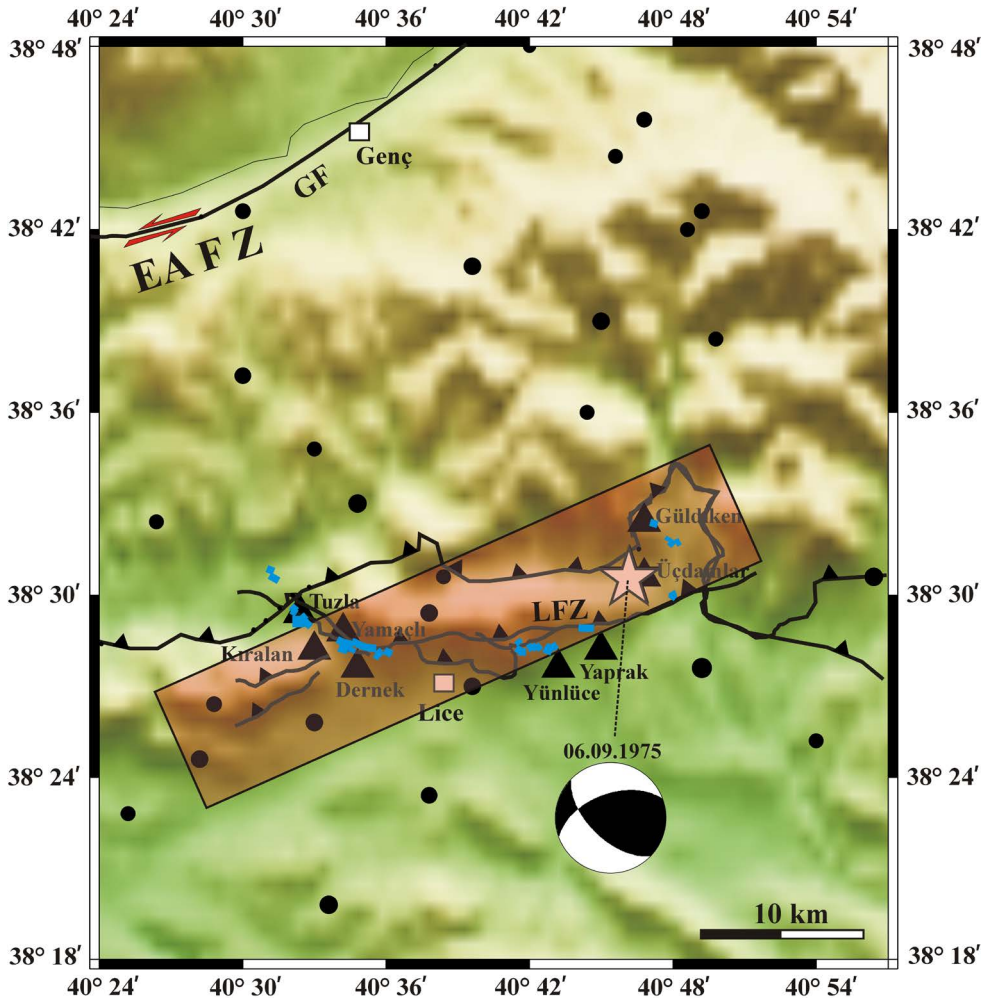

Figure 5. Location map showing the 1975 Lice earthquake's epicenter (star), source mechanism from Eyidoğan (1983), aftershocks (black circles) from Kalafat et al. (2007), surface ruptures (blue lines) mapped by Arpat (1977), and heavily damaged villages (black triangles)

6. Results of the Finite-Fault Analyses

A point-source grid consisting of 10 × 5 points (5 km spacing) along strike and dip, respectively, covering a rupture area of 45 km × 20 km, was used to represent the 1966 Varto earthquake faulting with rupture initiation at 6 km depth and 20 km from the SE edge (Fig. 6). The maximum rupture velocity is assumed to be 3.0 km/s. Five time windows were used for flexibility in rupture velocity. Slip rise times in each window were represented by an isosceles triangle with 2 s rise and fall times, with each window delayed by 2 s from the previous one. Notice that this parameterization for the 1966 Varto and the given parameterizations for the other studied earthquakes reflect the parameters selected after numerous inversions by checking against the calculated (the synthetic) waveforms with the observed waveforms (Tables S1-S4, Figs. S2-S5). Inversion runs with different faulting strike/dip angles and lengths/widths, rupture initiation points/velocities and rise times were carried. Different crustal velocity structures were also tested (Zor et al., 2003, 2006; Kahraman et al., 2015). The rake angle was allowed to vary within ±45° of the initially assigned value. The rake angle for the 1966 Varto earthquake was taken as 148°.

It is obtained that parameterization Model IRV11 in Table S1, requiring a southwest dipping rupture plane with rupture initiation depth of 6 km and velocity of 3.0 km/s, better explains the data. The finite-fault slip model resulting from the Model IRV11 is presented in Fig. 7. The slip distribution model yields a seismic moment of 1.63×10^{19} Nm ($M_W \approx 6.74$) and an average rake angle of 155°. A 3D representation of the slip model within the source region is provided in Fig. 8 for interpretation. The comparison between observed and synthetic waveforms from the best-fitting solution is also shown in Fig. 7. The model suggests the rupture occurred due to the failure of

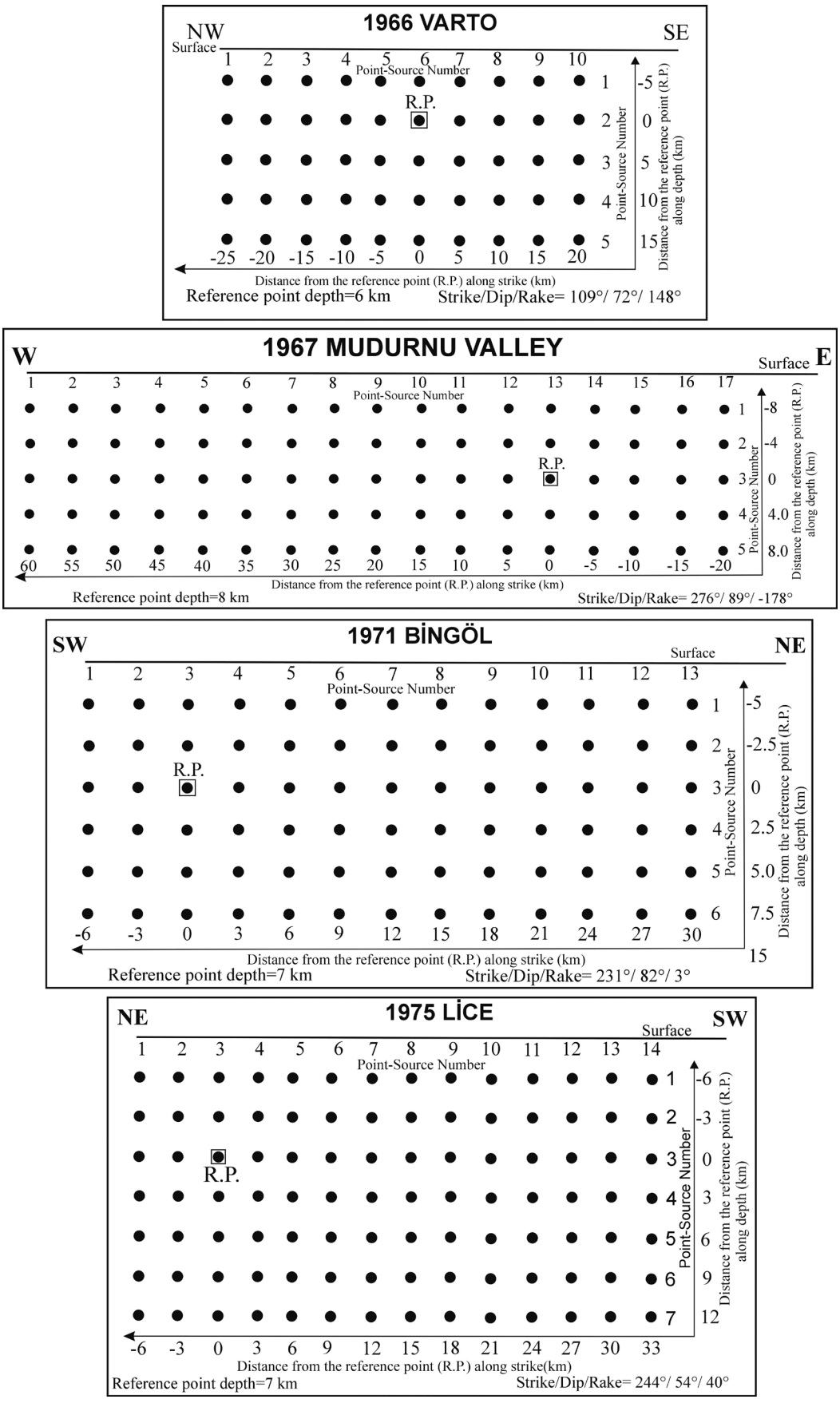

Figure 6. Schematic demonstration of the selected point source grid parameterizations used for the representation of the studied earthquakes' sources. See Tables S1-S4 for the other parameterizations. The reference point (R.P.) corresponds to the rupture initiation preferred by the data.

three asperities, with most of the seismic moment released from the rupture propagating northwestward. The largest asperity with a peak slip of 1.93 m located in the middle dominates the earthquake rupture and covers a rupture area of about 25 × 15 km^2 while the other asperities with much smaller peak slips (0.70 m and 0.67 m) and locations southeast and the northwest of the largest asperity, respectively. The results of the selected inversion trials are also given in Fig. S2.

Inversion runs carried out for the 1967 Mudurnu Valley earthquake are listed in Table S2 and depicted in Fig. S3 for some trials. The Model IRM17, in which the rupture is represented by a grid of 17 × 5 point sources with intervals of 5 km along strike and 4 km down dip and rupture initiation at a depth of 8 km and 20 km distance from the fault's eastern edge, is selected (Fig. 6). The strike, dip, and rake angles were set to 276°, 89°, and –178°, respectively. The maximum rupture velocity was set to 3.0 km/s. The point-source rise-time functions have equal rise and fall of 1.2 sn. The slip distribution model corresponding to the Model IRM17 is presented in Fig. 9, and the waveform comparison is shown in Fig. 10. This slip model suggests that the rupture is dominated by a large asperity with a maximum slip of about 6.0 m. The rupture initiated on this asperity and propagated primarily westward. A smaller asperity with about 2.8 meters of slip is located at the western end of the rupture at a slightly greater depth. The seismic moment is about 1.0 × 10^{20} Nm (M_W = 7.28), the average rake angle is 168°, and the total rupture length is 80 km.

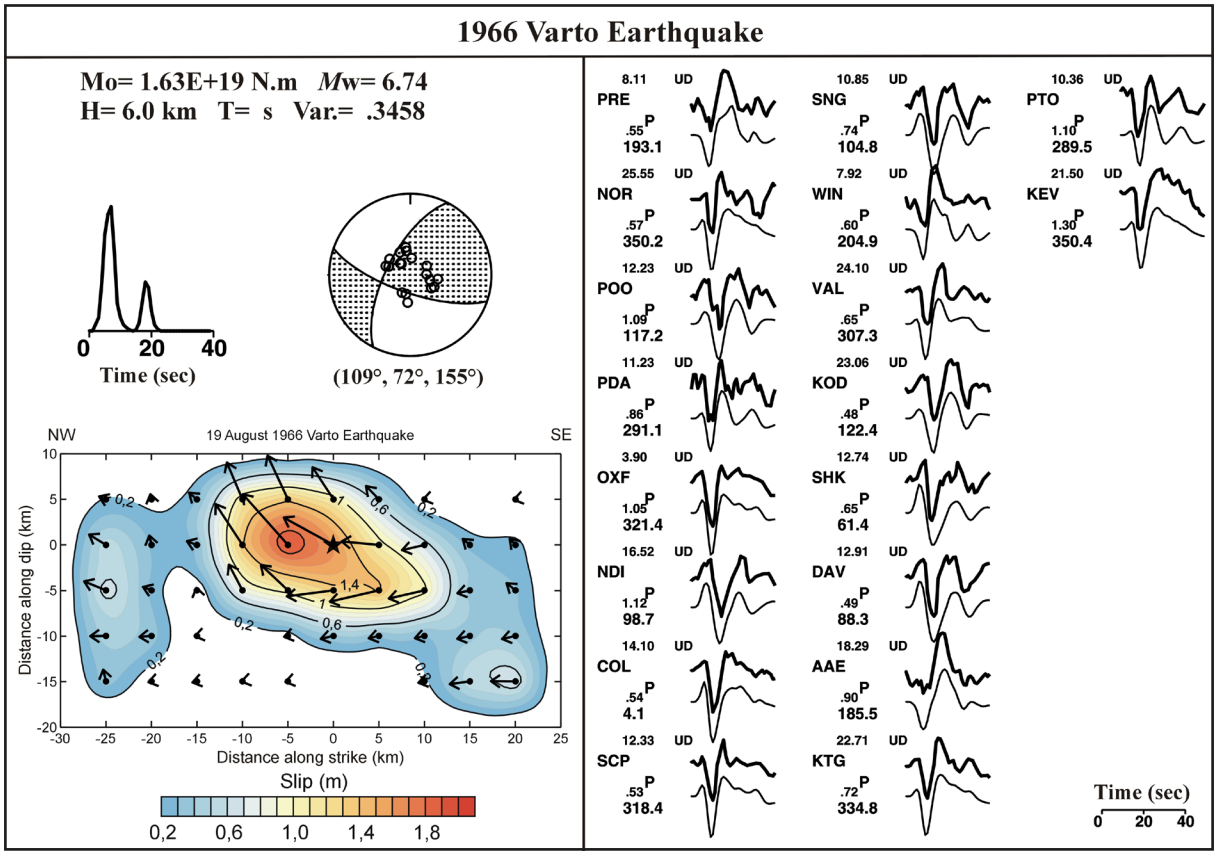

Figure 7. (Left) Results of the finite-fault inversion for the 1966 Varto earthquake and (right) comparison of the observed waveforms (thick lines) with synthetic waveforms (thin lines) calculated from the slip distribution model in the left. Seismic moment (M_O), variance (Var.), moment-rate function, source mechanism solution (grey-white focal sphere) and finite-fault slip model are given. Slips larger than 0.2 m are contoured with an interval of 0.2 m. The arrows on the slip model denote rake angles calculated for each point source, with length proportional to the slip amplitude. Comparison of the long-period P waveforms estimated for the slip model (thin grey lines) with observed waveforms (thick black lines) is shown on the right. The waveforms start at first P wave arrivals. Small numbers under the station names are peak-to-peak amplitude ratios, and large numbers are station azimuths. Numbers above the station names represent observed ground motions in microns. See Fig.S2 for comparison with the other models with different parameterizations.

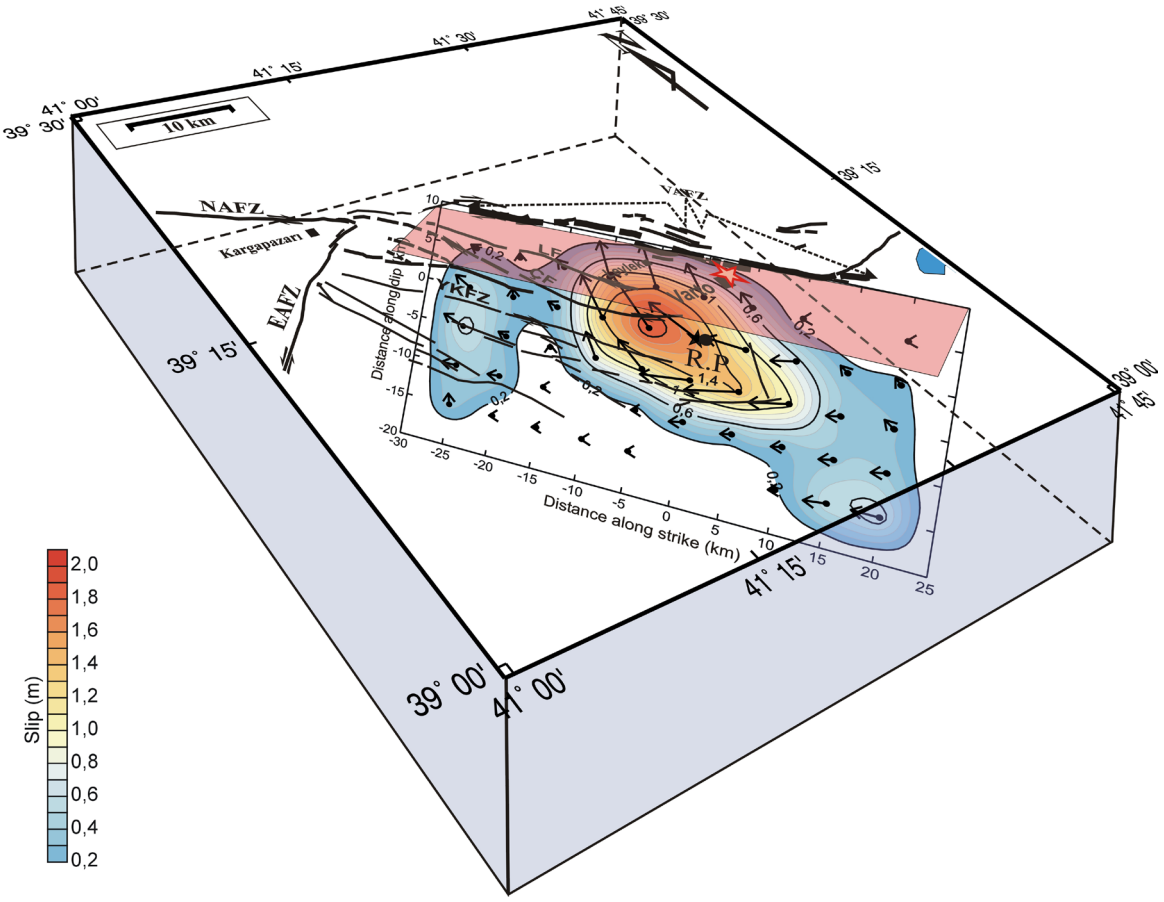

Figure 8. 3-D representation of the 1966 Varto earthquake source region with the finite-fault rupture model obtained in the study. See captions of Figs. 2 and 7 for the abbreviations.

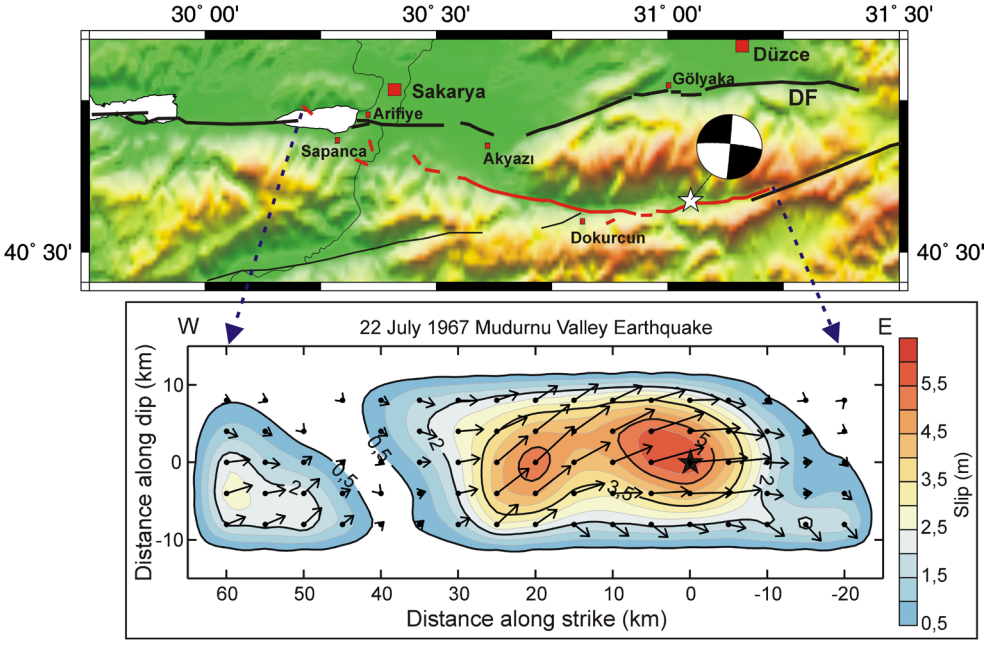

Figure 9. Computed slip distribution for the 1967 Mudurnu Valley earthquake and its comparison with the observed surface ruptures. Slip is contoured at 0.5 m intervals for values larger than 0.5 m. White and black stars show the epicenter and the reference point used in the inversion. See caption of Fig. 7 for the other explanations related to the slip model and Fig. S3 for comparison with the other models with different parameterizations. DF = Düzce Fault.

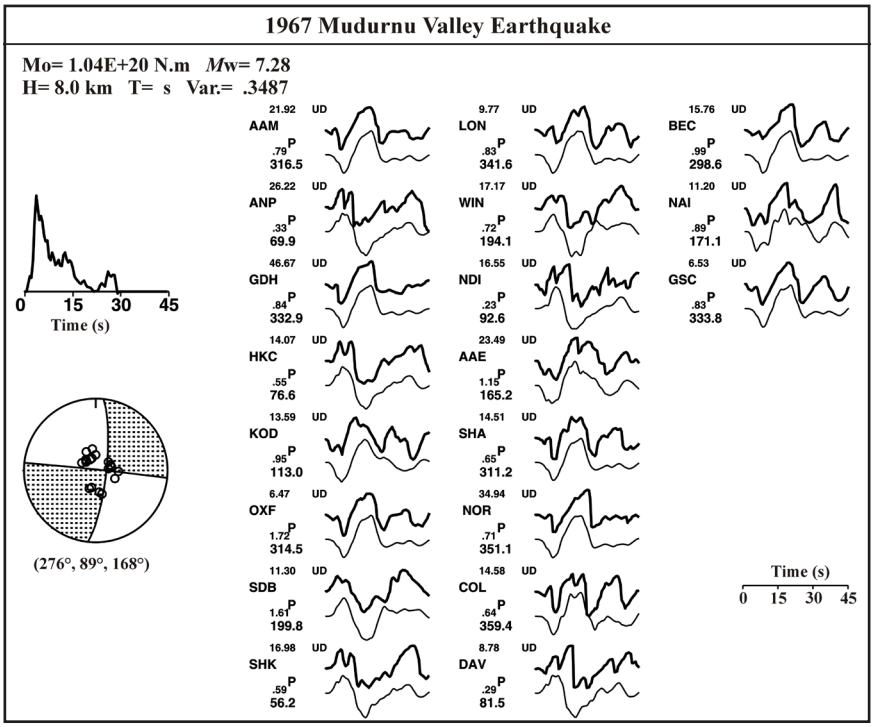

Figure 10. (Left) Results and (right) observed-synthetic waveform comparison for the finite-fault inversion of the 1967 Mudurnu Valley earthquake. See Fig. 9 for the slip distribution model and the caption of Fig. 7 for the abbreviations and explanations and Fig. S4 for comparison with the other models with different parameterizations.

For the finite-fault modeling for the 1971 Bingöl earthquake, a 13 × 6 point-source grid was used, with a strike of 231°, dip of 82°, and intervals of 3 km along strike and 2.5 km down dip, based on the surface ruptures and prior studies (Table 2, Fig. 4). The rake angle and rupture velocity were set to 3° and 3.0 km/s, respectively. The grid was placed such that the hypocenter (R.P.) was at a depth of 7 km, 6 km from the fault's southwestern edge. Based on the epicenter and surface ruptures, the rupture is interpreted to have propagated unilaterally northeastward (Table 2; Figs. 4 and 11a). Among the inversion trials carried out Model IRB6 trial with minimum variance value is selected for visualization of the results (Table S3; Figs. 11b and 12). The solution suggests that the rupture involves in failures of two asperities. The main, circular asperity covers the southwestern half of the fault plane, is centered on the hypocenter, and has a maximum slip of approximately 2.9 m. A smaller asperity, which covers deeper part of the northeastern half, has a maximum slip area with slip ranging 0.8-1.8 m. The slip distribution is consistent with the mapped surface rupture extent (Fig. 11). The rupture spanned ~40 km. The seismic moment is 1.44×10^{19} Nm, corresponding to $M_W = 6.71$. The results of the selected inversion trials are also visualized in Fig. S4.

A 39 km × 18 km point-source grid was defined, striking 244°, dipping 54°, and consisting of 98 points (14 along strike, 7 down dip, 3 km spacing) for the 1975 Lice earthquake (Fig. 6). The rupture initiation point (R.P.) was set at the third grid point in both directions, corresponding to a focal depth of 7 km, allowing slip to propagate to ~1 km depth. The initial rake angle and rupture velocity were 40° and 3 km/s, respectively. Five time windows were used, each with a slip rise time of 1.6 s (equal rise and fall), delayed by 0.8 s from the previous one, providing a total slip duration of 4.8 s per point source.

The slip distribution and waveform comparison for the selected solution with lowest variance value (Model IRL14 in Table S4) are shown in Fig. 13. The parameterizations and results for different models are given in Table S4 and Fig. S5. The average rake angle is 31°, and the seismic moment is 9.74×10^{18} Nm ($M_W \approx 6.6$). The model suggests the rupture was dominated by a major asperity and propagated unilaterally southwestward and mostly up-dip (Fig. 13). This asperity covers ~24 km × 15 km faulting area, and has a maximum slip of 0.75 m with a rake angle of 76°. The SW shallower section of the major asperity has slip and rake angle ranging 0.56-0.72 m and (−5)-19°, respectively. A smaller, deeper asperity is present near the southwestern edge, with dimensions of ~5 × 5 km², a maximum slip of ~0.3 m, and a rake angle ranging −5°-46°. The surface projection and a 3D representation of the model are shown in Fig. 14. The total rupture has a length of ~40 km and lasted for 18 s.

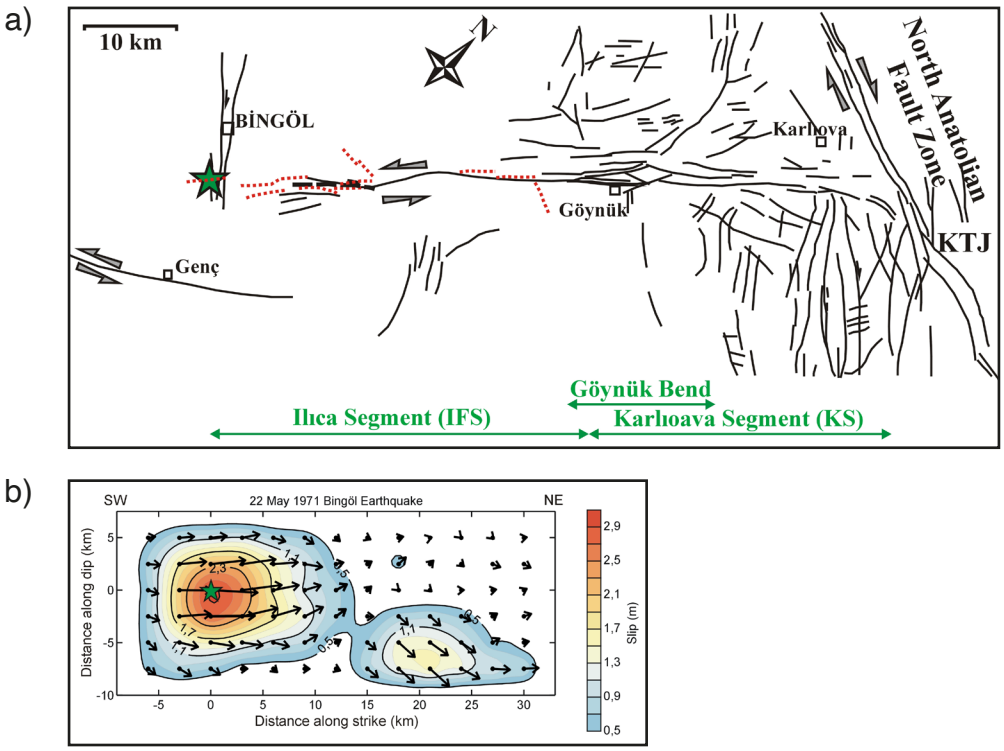

Figure 11. (a) Map of the Karlıova-Ilıca Fault Segment (Şaroğlu et al., 1992) with the 1971 Bingöl earthquake surface ruptures (red dashed lines) (Seymen and Aydın, 1972). (b) Calculated slip distribution for the 1971 Bingöl earthquake. Slip is contoured at 0.2 m intervals for values larger than 0.5 m. Green stars show the epicenter and rupture initiation point. See caption of Fig. 7 for the other explanations related to the slip model.

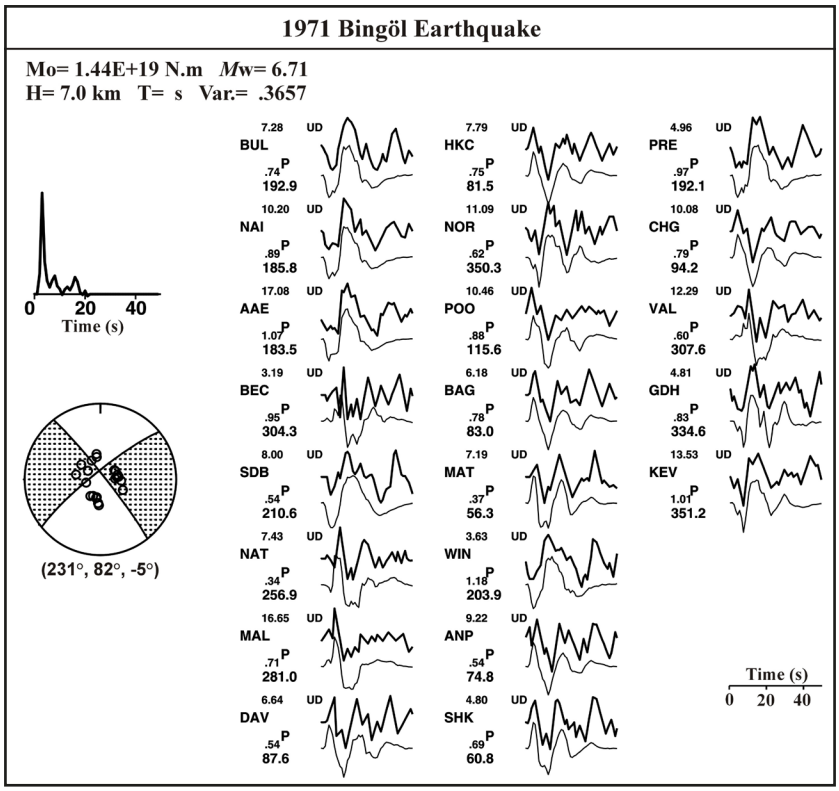

Figure 12. (Left) Results and (right) observed-synthetic waveform comparison for the finite-fault inversion of the 1971 Bingöl earthquake. See Fig. 11b for the slip distribution model and caption of Fig. 7 for the abbreviations and explanations.

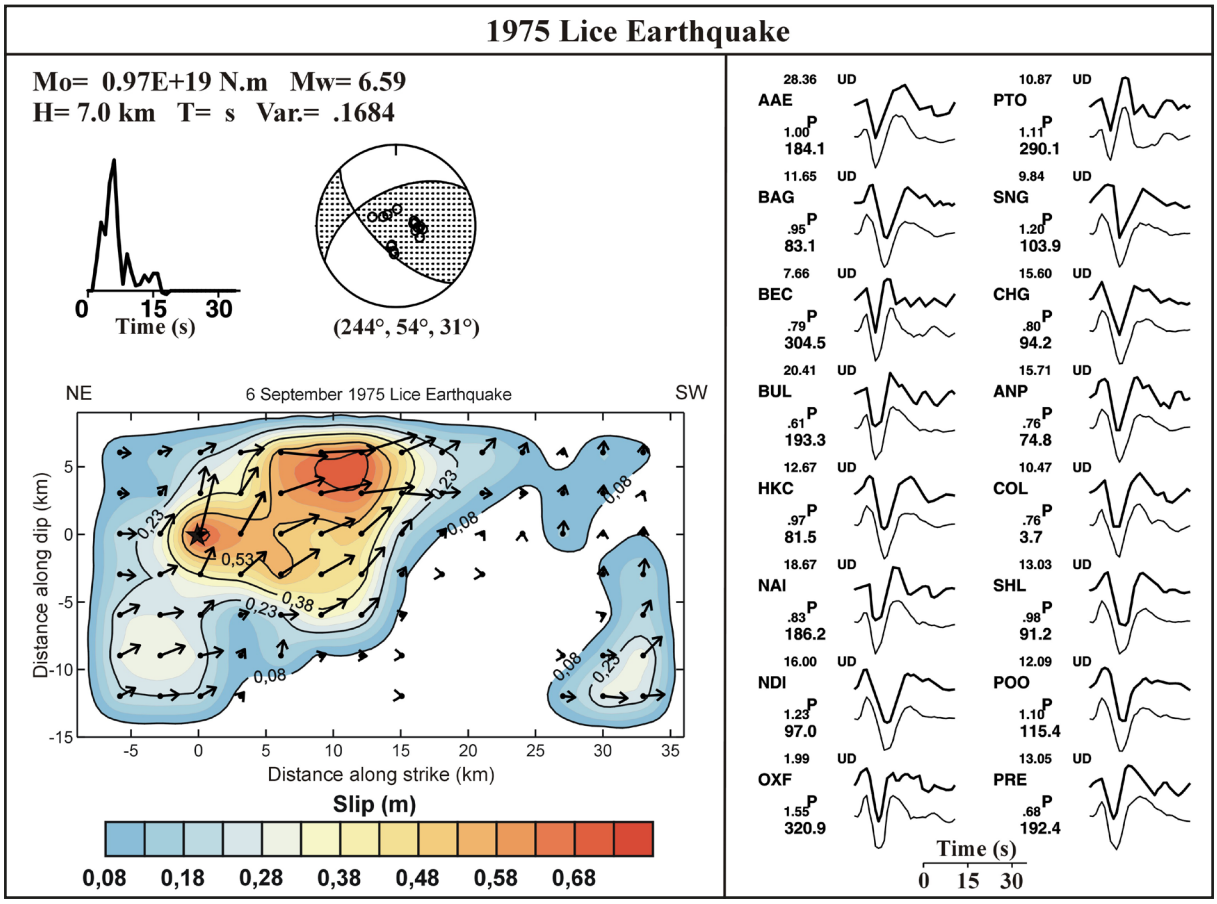

Figure 13. (Left) Results of the finite-fault inversion for the 1975 Lice earthquake and (right) comparison of observed waveforms (thick lines) with synthetic waveforms (thin lines). Slips larger than 0.08 m are contoured at 0.15 m intervals. See caption of Fig. 7 for the abbreviations and explanations and Fig. S5 for comparison with the other models with different parameterizations.

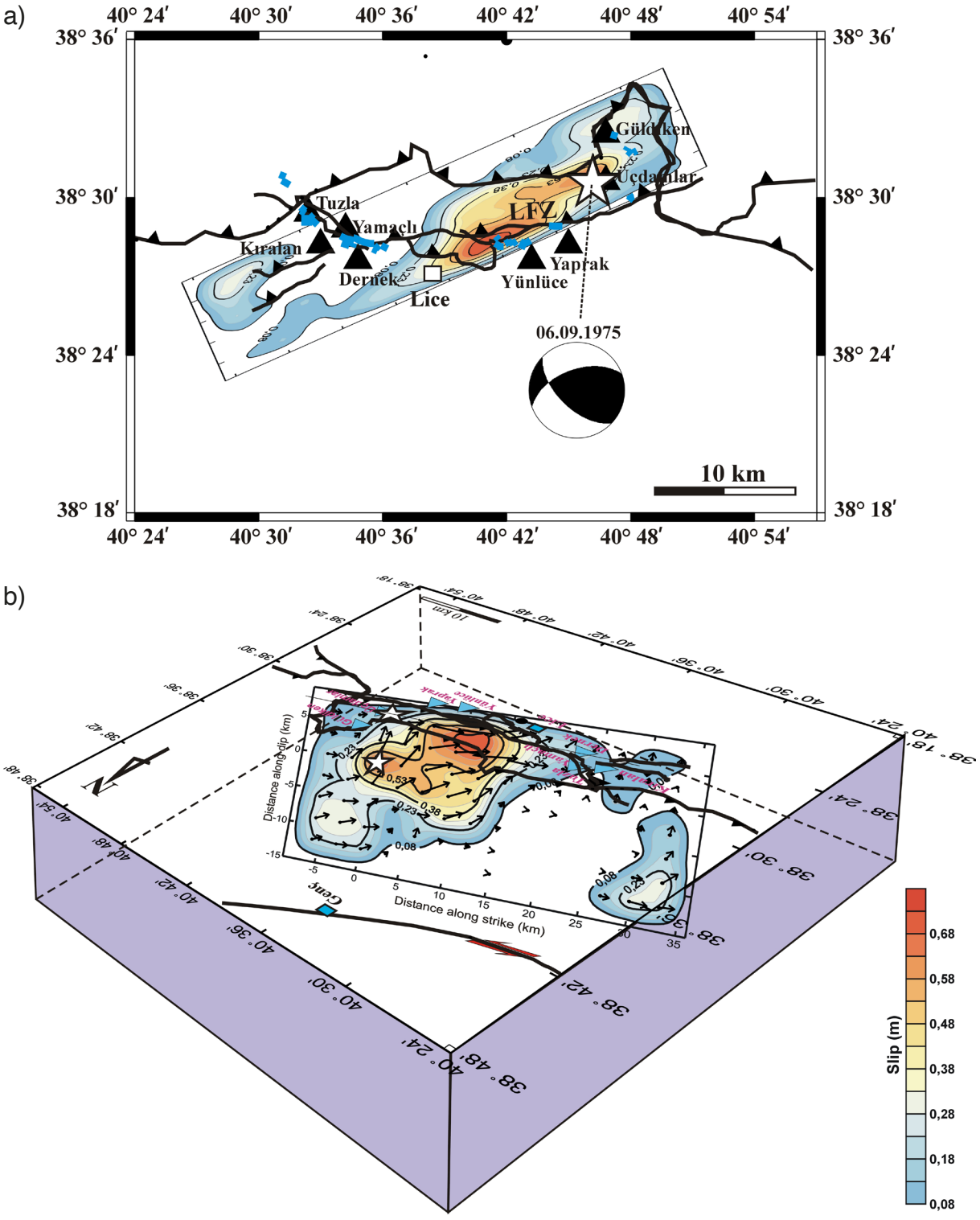

Figure 14. (a) Surface projection of the finite-fault model for the 1975 Lice earthquake. Blue lines represent the earthquake's surface ruptures (b) 3D representation of the source region with the obtained rupture model. White stars denote the epicenter/hypocenter; blue triangles denote heavily damaged villages.

7. Discussion

The finite-fault slip model presented in Figs. 7 and 8 suggests that the rupture of the 1966 Varto earthquake initiated on the largest asperity having a peak slip (~1.9 m) area located approximately 5 km west of the hypocenter. Rake angles over the higher slip areas range between 123° and −167, with 132° for the peak slip location, indicating

oblique faulting. The rake angle corresponding to overall rupture is 155°. Rupture initiation at 6 km depth and rupture velocity of 3.0 km/s gives a much better fit to the data (Table S1). In general, the largest asperity and SE asperity appear in all inversion trials (Fig. S2). However, the NW asperity becomes apparent for longer rise times, implying relatively longer slip duration or slower rupture velocity for that part of the faulting. Additionally, as the rupture velocity increases, this asperity becomes deeper and higher in slip amplitude, while lower rupture velocities require lower and shallower slips in the shorter rupture models, suggesting more rupture length toward NW. Use of a longer rupture plane by assigning a point source interval of 5 km increased to fit to data (compare Models IRV6 and IRV11 in Table S1). The inversion trials suggest that the maximum slip is around 2.0 m.

The selected rupture model (Model IRV11 in Table S1) indicates that the 1966 Varto earthquake resulted from oblique faulting along the VAFZ, which comprises two segments with dominant right-lateral strike-slip and reverse components (Figs. 7 and 8; Wallace, 1968; Pınar, 1995; Emre et al., 2013). This interpretation is consistent with the identification of a transpressional zone east of the KTJ by Sançar et al. (2015). Emre et al. (2013) reported that both fault segments had been ruptured by the earthquake. It is noteworthy that the rupture initiation near the region of maximum slip coincides with a right-stepping fault jog between the two segments, suggesting that this geometric discontinuity influenced the rupture process. The rupture on the small southeastern asperity further suggests that the rupture propagated eastward for an additional ~10 km beyond the largest asperity (Figs. 4 and 5).

There is disagreement regarding the dip direction of these segments. Gürboğa (2015) shows both segments dipping to southwest, while Karaoğlu et al. (2017) depict the northwestern segment as near vertical and the southeastern segment dipping northeast. Although a focal mechanism solution by Stewart and Kanamori (1982) indicates a dip of 65° to the northeast, the waveform inversion by Pınar (1995) suggests a dip of 72° to the southwest (Table 2). Our inversion trials for both scenarios found that the model with a southwest-dipping fault provided a significantly better fit to the observed data (compare Models IRV1 and IRV2 in Table S1, Fig. S2).

For the 1967 Mudurnu Valley earthquake, the results of the all inversion trials with different parameterizations require a large asperity, whose rupture mostly propagated west from the hypocenter with peak slip mostly above 4 m, and a smaller asperity, whose rupture remained at depth near the western edge of the faulting, with peak slip mostly above 2.5 m (Table S2, Figs. 9 and S3). These general characteristics of the rupture are well preserved in parametrizations with different point source intervals and rupture velocities (Fig. S3). A larger rupture velocity (3.3 km/s) gives a degraded fit to data while the slower rupture velocities (2.7 and 2.4 km/s) do not significantly improve the fit. As the time window approach allows slower rupture velocities than the selected maximum rupture velocity, we select a maximum rupture velocity of 3.0 km/s. The inversion trials demonstrate that about 60 km rupture propagation toward the west is demanded by the data. The point-source grids striking more northwest (models IRM9 and IRM10 in Table S2) give a significantly poor fit to the data, suggesting that the main rupture with dominant seismic moment release occurred along the eastern part of the faulting with roughly East-West strike.

A paleoseismological study (Palyvos et al., 2007) along the rupture indicated a paleoearthquake after 1693. Although this paleoearthquake was not confidently related to any of the historical events that occurred post 1693, it might have been either the 1668 North Anatolian or the 1719 İzmit earthquakes (Ambraseys and Finkel 1988; Stein et al., 1997; Fraser et al., 2009; Hartleb et al., 2003; Palyvos et al. 2007; Kozacı et al., 2011). This means that 248-299 years passed from penultimate earthquake to the 1967 Mudurnu Valley earthquake. The time span is comparable to the earthquake recurrence time of 330-370 years proposed for the 1999 Düzce earthquake fault segments, shown as Düzce Fault in Fig. 3a, lying parallel in the north (Pantosti et al., 2008). The slip rate along the 1967 and the 1999 fault segments were calculated 12 and 15.0 ± 3.2 mm/year fom the GPS and the geologic field data, respectively (Pondard et al., 2007; Pucci et al., 2008). Given the slip rate and the time interval after the penultimate earthquake, slip as much as 4.5 m accumulated along the 1967 fault segment, coinciding with peak slip mostly above 4 m found in the inversion trials for the larger asperity. Additionally, Akyüz et al., (2002) measured a maximum 5 m slip along the 1999 Düzce earthquake's surface rupture, while Konca et al., (2010) obtained peak slip as much as 7 m from the joint inversion of the seismological and geodetic data. Therefore, greater slip (4-6 m) obtained at depth obtained from the inversions than measured at surface (e.g. 2 m) is considered reasonable.

The section of the 1967 fault containing the large asperity's higher slip areas is roughly E-W oriented (Fig. 9). Approximately 19 km west of the hypocenter, the fault strike gradually changes by 20 degrees to a NW-SE orientation, forming a bend. Beyond this bend, slip amplitudes on the large asperity decrease from 5.4 m to below 1 m toward the west. Use of both different rupture velocities and slip rise-times in the trials also implicate a relative rupture slowing down along and after crossing the bend (Table S2; Fig. S3). This indicates that the 20-degree fault bend

created a geometric discontinuity that influenced rupture propagation, a phenomenon also observed during the 1857 Fort Tejon earthquake on the San Andreas Fault (Sieh, 1978). The rupture terminates at a structural discontinuity formed by its intersection with faults that later generated the 1999 İzmit earthquake. In this region, a small asperity is located at depth, correlating with reported vertical surface displacements (Ambraseys and Zatopek, 1969; Muller et al., 2003). The largest aftershock, which exhibited a normal faulting mechanism (McKenzie, 1972), occurred in this area (Dewey, 1976) and may have resulted from the rupture of shallower sections above this asperity. It is also noteworthy that the 1967 rupture overlaps with the 1957 Abant earthquake rupture for about 20 km at its easternmost section (Figs. 1 and 9) (Ambraseys and Zatopek 1969; Barka 1996). Notice that the 1967 rupture model requires almost no slip for shallower part of the overlapping faulting for 10 km.

Regarding the inversion trials for the 1971 Bingöl earthquake with varying parameterizations, the rupture of two asperities (a large one over the SW and the smaller one over the NE halves of the fault plane) with peak slip in the range 2.0-3.0 m is a robust feature (Table S3; Figs. 11b and S4). The rupture initiation at a shallow depth of 7 km and

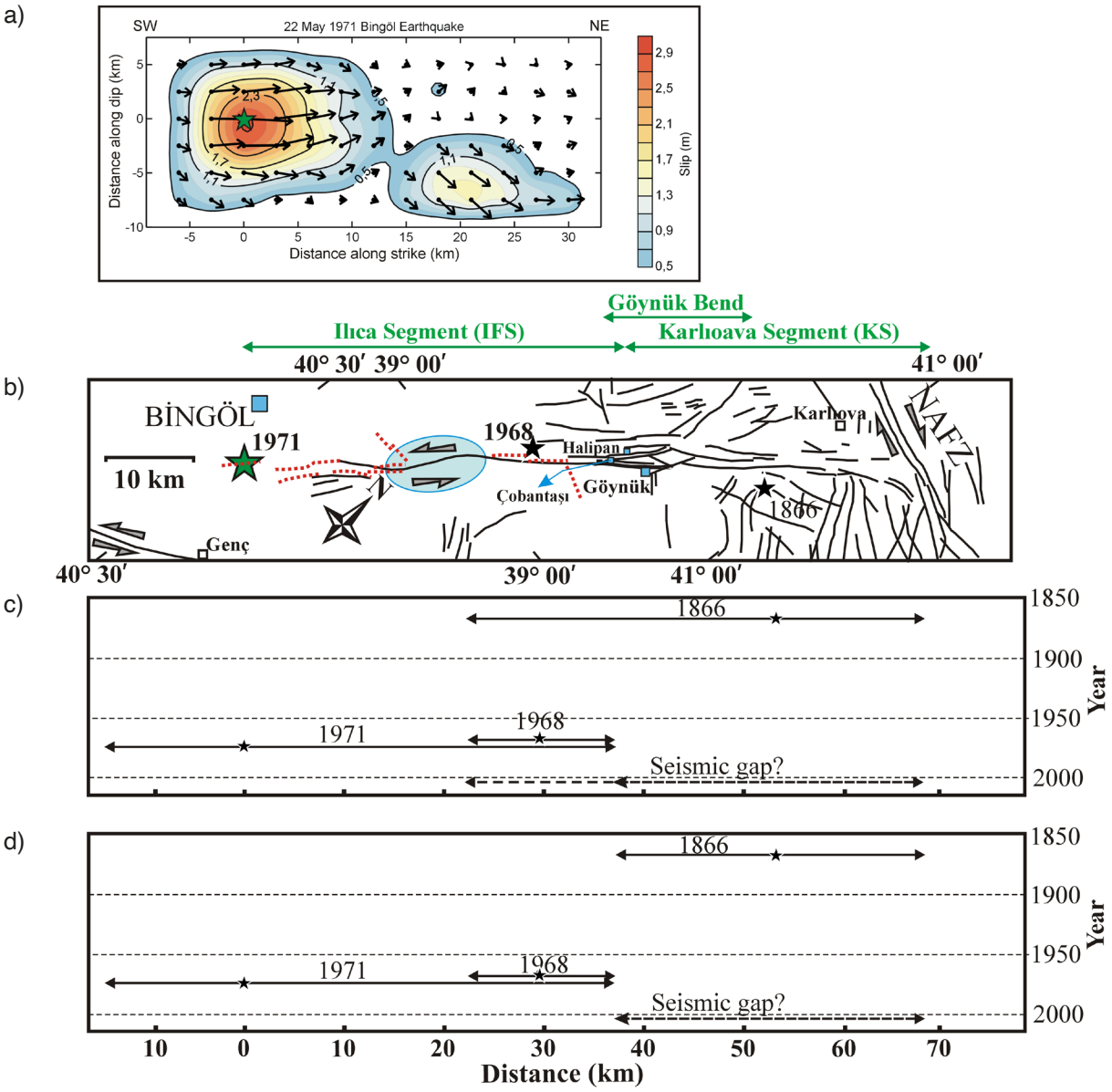

Figure 15. (a) The finite-fault model obtained for the 1971 Bingöl earthquake, (b) the map view of the Karlıova Ilıca Fault Segment and its subsections (compiled from Seymen and Aydın (1972), Ambraseys (1997) and Duman and Emre (2013)) and (c), (d) possible earthquake occurrence models after the 1866 earthquake. The stars indicate earthquake epicenters, and the transparent blue ellipse shows the geometric fault discontinuity discussed in the study.

a rupture length of ~40 km are clearly preferred by the data (Models from IRB1 to IRB3 in Table S3). The data is also best explained by a rupture velocity of 3.0 km/s (Models from IRB6 to IRB 10 in Table S3). The total rupture duration is 20 s, about two-thirds of which constitutes moment release of the larger asperity (Fig. 10). Another conspicuous property is that the normal component of the faulting becomes prominent over the high slip area of the smaller asperity, suggesting a possible effect of the Göynük Bend (Figs. 11 and S4).

The 1971 Bingöl earthquake's slip distribution model supports the segmentation of the East Anatolian Fault Zone (EAFZ) at the Göynük Bend, contradicting the single-segment model proposed by Barka and Kadinsky-Cade (1988) and used by Utkucu et al. (2003) (Fig. 11). Historical evidence (Ambraseys, 1997) and structural mapping (Duman and Emre, 2013) indicate that the KS likely ruptured during the 1866 Göynük earthquake, while the 1971 event ruptured the IFS (Figs. 15a,b). Our model confirms the 1971 rupture was confined to the IFS and did not propagate northeastward beyond the Göynük Bend, an interpretation supported by the termination of surface ruptures (Seymen and Aydın, 1972) and the extent of high-intensity shaking (Fig. 4). The 1866 Göynük earthquake is interpreted to have ruptured the KS. Historical sources reported that the 1866 Göynük earthquake produced surface ruptures that began in the village of Halipan (present-day Derinçay or Halifan) within the Göynük Bend and extended continuously toward the KTJ for a walking distance of approximately 8 hours (Fig. 15b; Ambraseys, 1997). Ambraseys (1997) proposed the walking distance to be about 45 km. However, the 45 km rupture length inferred from historical accounts (Ambraseys, 1997) appears to be an overestimate given the segment's 32 km length; the affected intensity area likely includes the northern IFS, suggesting the 1866 event may have been larger.

The 1968 Göynük earthquake ($M_S = 6.3$) occurred on the northern IFS, with its epicenter located above our model's smaller asperity (Figs. 4, 15a and 15b; Dewey, 1976). The slip deficit between the large and small asperities is consistent with the occurrence of the 1968 event on the northern part of the IFS. A change in fault strike between the large and small asperities suggests a geometric discontinuity within the IFS itself, implying it may be composed of two sub-segments. While this discontinuity may not act as a major barrier to large earthquake ruptures-unlike the Göynük Bend-it nonetheless influences rupture characteristics. Additionally, the location of the large asperity and some observed surface ruptures requires that the IFS extend southwestward beneath the sediments of the Bingöl Plain in the east of the city center (Figs. 15a and 15b).

The KS, having accumulated strain for ~160 years at geodetic slip rates of 8-11 mm/yr (Reilinger et al., 2006; Walters et al., 2014; Vernant, 2015; Aktuğ et al., 2016; Özbakır et al., 2017), represents a significant seismic gap with cumulative deformation of approximately 1.3-1.7 meters. Assuming uniform deformation accumulation and no significant creep along the 32-km-long KS within the seismic gap, a seismic moment equivalent to the 1971 Bingöl earthquake has likely accumulated.

Two possible rupture scenarios post-1866 are proposed for the KIFS (Figs. 15c and 15d), depending on the historical extent of that event. If, as suggested by Ambraseys (1997), the 1866 rupture extended over approximately 45 km, then the rupture must have propagated into the proposed northern sub-segment of the IFS, which also hosted the 1968 Göynük earthquake (Fig. 15c). This would mean that a 45-km-long section of the EAFZ currently constitutes a seismic gap. However, historical accounts indicate that surface ruptures began at Halipan village as pointed out above (Fig. 15b) (Ambraseys, 1997). In that case, the 1866 earthquake was likely generated solely by the 32-km-long KS (Fig. 15d). The northern section of the IFS seems to generate relatively small independent events or may be part of longer ruptures of the larger events, such as the 1971 Bingöl earthquake. A comparable rupture pattern has also been observed in Southern California, during the 1940 ($M_W = 7.0$) and 1979 ($M_W = 6.4$) Imperial Valley earthquakes (Sieh, 1996), where the latter event occurred due to the re-rupture of a fault section that had experienced relatively lower slip during the earlier event.

Finally, for the 1975 Lice earthquake, the major asperity corresponds to the rupture of the LF and its rupture is arrested by a western fault step-over, constituting a geometric barrier (Fig. 14). This finding provides seismological evidence supporting King and Nabelek's (1985) interpretation that a step-over beneath Dernek, Kıralan, Yamaçlı and Tuzla villages stopped the rupture (Figs. 5 and 14a). No matter which parameterization is used, the major asperity appears in all the resulting rupture models with roughly similar rupture area and peak slip, mostly between 0.6-1.0 m (Table S4, Figs. 13 and S5). Though a slip over the minor asperity exists in all rupture models, its amplitude is as low as ~0.1 m in some models, making its presence as an asperity vague. Nevertheless, the existence of some slip beneath the western fault step-over in all rupture models supports the interpretation that the rupture may have attempted to jump across the barrier, consistent with mapped surface ruptures (Figs. 5 and 14a). The no-slip area between the asperities further supports this reckoning. Earlier waveform studies (Eyidoğan, 1980, 1983; Pınar, 1995) identified sources corresponding to our major asperity but did not report the minor one. Another interesting

point is that the data strongly prefer a shallow rupture initiation point at 7 km depth (inversion trials from Model IRL1 to IRL4 in Table S4) with rupture velocity below 3.3 km/s (inversion trials from Model IRL4 to IRL8 in Table S4). The best fit to the data is achieved for a rupture velocity of 3.0 km/s.

Kahraman et al. (2015) derived the crustal structure beneath the western part of the 1967 Mudurnu Valley earthquake rupture using a dense broadband seismic station network and receiver function analysis. Zor et al. (2006) determined the velocity structure beneath a station in close proximity to the 1967 earthquake rupture using the same analysis. Both velocity models were tested in the inversion of the 1967 earthquake (Models IRM22 and IRM23 in Table S2). These tests resulted in larger variance values but produced similar slip distribution models that differ in detail. Inversion trials using a different crustal velocity model (Zor et al., 2003) were also performed for the other earthquakes. For these earthquakes, similar rupture models were obtained that differ in detail but exhibit a poorer fit to the data (Models IRV14, IRB13, and IRL16 in Tables S1, S3, and S4, respectively).

Overall, the findings of this study provide robust seismological evidence supporting the complex nature of earthquake rupture processes and the fundamental influence of fault discontinuities. As indicated in earlier studies (King and Nabelek, 1985; Sibson, 1985, 1987; Barka and Kadinsky-Cade, 1988; Barka, 1996), step-overs, bends, and segment boundaries act critically in controlling, initiating, perturbing, or arresting earthquake ruptures. The kinematic and dynamic rupture models derived from the high-quality seismologic and geodetic data for recent earthquakes along the NAFZ and EAFZ, together with dynamic rupture simulations, also support these findings (Oglesby and Mai 2012; Wang et al., 2023; He et al., 2025). For all studied earthquakes, the ruptures initiated on or close to the areas of highest slip, consistent with the results of Mai et al. (2006), who used numerous kinematic finite-fault slip models, and Oglesby and Mai (2012), who implemented spontaneous dynamic rupture simulations for scenario earthquakes along the NAFZ beneath the Sea of Marmara. These studies indicate that hypocenters are preferentially located near high-slip areas along ruptured faults.

8. Conclusions

This study successfully derived finite-fault rupture models for four significant historical earthquakes in Türkiye using teleseismic P-waveform inversion. The models provide detailed insights into the slip distribution, asperity patterns, and rupture processes of these events, consistently highlighting the paramount influence of pre-existing structural complexities on earthquake rupture dynamics.

The 1966 Varto earthquake is modeled as an oblique rupture involving three asperities, with its initiation point coinciding with a right-stepping fault jog. The 1967 Mudurnu Valley earthquake rupture was dominated by a large asperity, with its propagation and termination controlled by a 20-degree fault bend and its intersection with the future 1999 İzmit rupture zone, respectively. For the 1971 Bingöl earthquake, the slip distribution confirms that the rupture is confined to the IFS and do not propagate northeast through the Göynük Bend, reinforcing the segmentation of the EAFZ and identifying the adjacent KS as a potential seismic gap. The rupture model also suggests the IFS itself is composed of sub-segments, bounded by a geometric discontinuity that aligns with the northeastern edge of the main asperity. Finally, the model for the 1975 Lice earthquake provides seismological evidence for rupture arrest at a fault step-over, supporting earlier interpretations based on geological observations.

Collectively, these findings demonstrate that fault bends, step-overs, and segment boundaries act as critical controls on earthquake rupture, often serving as initiation points or barriers that halt propagation. The detailed finite-fault models presented here not only enhance our understanding of these specific historical events but also provide valuable constraints for improving seismic hazard models and understanding earthquake recurrence patterns in Türkiye's complex tectonic environment.

CRediT authorship contribution statement. Conceptualization: MU, ŞB; Methodology: MU, ŞB, FU; Formal analysis and investigation: MU, ŞB, FU, HD, SSN; Visualization: MU, ŞB, HD, FU; Writing-original draft preparation: MU, SSN; Writing-review and editing: MU, SSN, FU, HD.

Declaration of competing interest. The authors declare that they have no known competing financial interests or personal relationships that could have influenced the work reported in this paper.

Acknowledgements. This study was funded by The Scientific and Technological Research Council of Türkiye (TÜBİTAK) (project number: 121Y271) and partly benefited from the MSc thesis of one of the authors (Ş. Berzah). The figures were generated using the Generic Mapping Tools (GMT) developed by Wessel and Smith (1998) and Surfer 13 plotting software. The authors extend special thanks to Dr. Ali Pınar, who digitized and provided long-period teleseismic recordings used in the study. The authors also extend their thanks to the editor, Ilaria Spassiani, for handling the review process efficiently, and to the reviewers for their constructive comments, which significantly improved the quality of the manuscript.

References

Aktug, B., J. M. Nocquet, A. Cingöz et al. (2009). Deformation of western Turkey from a combination of permanent and campaign GPS data: Limits to block-like behavior, J. Geophys. Res.: Solid Earth, 114, B10404, doi:10.1029/2008JB006000.

Aktuğ, B., H. Ozener, A. Dogru et al. (2016). Slip rates and seismic potential on the East Anatolian Fault System using an improved GPS velocity field, J, Geodyn., 94, 1-12, doi:10.1016/j.jog.2016.01.001.

Akyüz, H. S., R. Hartleb, A. Barka, E. Altunel et al. (2002). Surface Rupture and Slip Distribution of the 12 November 1999 Düzce Earthquake (M 7.1), North Anatolian Fault, Bolu, Turkey, Bull. Seism. Soc. Am., 92, 1, 61-66.

Alptekin, Ö., J. L. Nabelek and M. N. Toksöz (1986). Source mechanism of the Bartın earthquake of September 3, 1968 in northwestern Turkey: evidence for active thrust faulting at the southern Black Sea margin, Tectonophysics, 122, 73-88.

Ambraseys, N. N. and C. F. Finkel (1988). The Anatolian Earthquake of 17 August 1668, in Historical Seismograms and Earthquakes of the World, 173-180. Eds. Lee, W. H. K., Meyers, H. and Shimazaki, K., Academic Press.

Ambraseys, N. N. and A. Zatopek (1967). The Varto Üstükıran (E.Anatolia) earthquake of 19 August 1966. A field report WS/0267, 81-AVS Paris, February 1967, UNESCO.

Ambraseys, N. N. and A. Zatopek (1968). The Varto Üstükıran (Anatolia) earthquake of 19 August 1966 summary of a field report, Bull. Seism. Soc. Am., 58, 1, 47-102, doi:10.1785/BSSA0580010047.

Ambraseys, N. N. and A. Zatopek (1969). The Mudurnu Valley, west Anatolia, Turkey, earthquake of 22 July 1967, Bull. Seism. Soc. Am., 59, 521-589, doi:10.1785/BSSA0590020521.

Ambraseys, N. N. (1988). Engineering seismology, Earthquake Engineering and Structural Dynamics, 17, 1-105.

Ambraseys, N. N. (1989). Temporary seismic quiescence: SE Turkey, Geophys. J. Int., 96, 2, 311-331.

Ambraseys, N. N. (1997). The little-known earthquakes of 1866 and 1916 in Anatolia (Turkey), J. Seismol., 1, 289-299.

Ambraseys, N. N. (2001). Reassessment of earthquakes, 1900-1999, in the Eastern Mediterranean and the Middle East, Geophy. J. Int., 145, 2, 471-485, doi:10.1046/j.0956-540x.2001.01396.x.

Ambraseys, N. N. and J. A. Jackson (1998). Faulting associated with historical and recent earthquakes in the Eastern Mediterranean region, Geophys. J. Int., 133, 2, 390-406, doi:10.1046/j.1365-246X.1998.00508.x.

Arpat, E. and F. Şaroğlu (1972). Doğu Anadolu fayı ile ilgili bazı gözlemler ve düşünceler. MTA Enstitüsü Dergisi, 78, 44-50.

Arpat, E. (1977). 1975 Lice Depremi., Yeryuvarı ve İnsan, 2, 1, 15-27.

Barka, A. and K. Kadinsky-Cade (1988). Strike-slip fault geometry in Turkey and its influence on earthquake activity, Tectonics, 7, 663-684, doi:10.1029/TC007i003p00663.

Barka, A. (1996). Slip distribution along the North Anatolian Fault associated with the large earthquakes of the period 1939 to 1967, Bull. Seism. Soc. Am., 86, 1238-1254, doi:10.1785/BSSA0860051238.

Beresnev, I. A. and G. M. Atkinson (1997). Modeling finite fault radiation from ω^n spectrum, Bull. Seism. Soc. Am. 87, 67-84, doi:10.1785/BSSA0870010067.

Beresnev, I. A. and G. M. Atkinson (1998). FINSIM – A FORTRAN program for simulating stochastic acceleration time histories from finite faults, Seism. Res. Lett., 69, 27-32, doi:10.1785/gssrl.69.1.27.

Berzah, Ş. (2018). 19 Ağustos 1966 Varto (Ms = 6.8) ve 6 Eylül 1975 Lice (Ms = 6.6) depremleri için telesismik sonlu-fay modellerinin belirlenmesi, Master Thesis, Sakarya University.

Boore, D. M. (2009). Comparing Stochastic Point-Source and Finite-Source Ground-Motion Simulations: SMSIM and EXSIM, Bull. Seism. Soc. Am. 99, 6, 3202-3216, doi:10.1785/0120090056.

Canıtez, N. (1972). Source mechanism and rupture propagation in the Mudurnu Valley (Turkey) earthquake of July 22, 1967, Pure Appl. Geophys., 93, 116-124.

Copley, A. and J. Jackson (2006). Active tectonics of the Turkish-Iranian Plateau, Tectonics, 25, TC6006, doi:10.1029/2005TC001906.

Dewey, J. W. (1976) Seismicity of northern Anatolia, Bull. Seism. Soc. Am., 66, 843-868, doi:10.1785/BSSA0660030843.

Duman, T. and Ö. Emre (2013). The East Anatolian Fault: geometry, segmentation and jog characteristics, Geol. Soc. 372, 495-529, doi:10.1144/SP372.1.

Emre, Ö., T. Y. Duman, S. Özalp et al. (2013). Active fault map of Turkey with explanatory text 1:1.250.000 scale, Special Publication Series-30, General Directorate of Mineral Research and Exploration. Turkey, ISBN: 978-605-5310-56-1.

Eyidoğan, H. (1980). The source parameters of the Lice, Turkey earthquake of September 6, 1975, In individual studies by partipicants at IISEE 16, 107-103.

Eyidoğan, H. (1983). Bitlis-Zağros bindirme ve kıvrımlı kuşağının sismotektonik özellikleri. PhD Thesis, İstanbul Technical University.

Eyidoğan, H., Z. Utku, U. Güçlü and E. Değirmenci (1991). Türkiye büyük depremleri makro-sismik rehberi 1900-1988, İstanbul Teknik Üniversitesi Maden Fakültesi Jeofizik Bölümü Yayınları, İstanbul.

Eyidoğan, H., S. S. Nalbant, A. Barka and G. C. P. King (1999). Static stress changes induced by the 1924 Pasinler (M = 6.8) and 1983 Horasan-Narman (M = 6.8) earthquakes, Northeastern Turkey, Terra Nova, 11, 38-44.

England, P., G. Houseman and J. M. Nocquet (2016). Constraints from GPS measurements on the dynamics of deformation in Anatolia and the Aegean, J. Geophys. Res.: Solid Earth, 121, 8888-8916, doi:10.1002/2016JB013382.

Graves, R. W. (1998). Three-Dimensional Finite Difference Modeling of the San Andreas Fault: Source Parameterization and Ground Motion Levels, Bull. Seism. Soc. Am. 88, 881-897, doi:10.1785/BSSA0880040881.

Gürboğa, Ş. (2015). Source fault of 19 August 1966 Varto earthquake and it's mechanism: New field data, Eastern Turkey. J. Asian Earth Sci., 111, 792-803, doi:10.1016/j.jseaes.2015.07.015.

Hall, J. F., T. H. Heaton, M. W. Halling and D. J. Wald (1995). Near-source ground motion and its effect on flexible buildings, Earthquake Spectra, 11, 569-605, doi:10.1193/1.1585828.

Hartzell, H. S. and T. H. Heaton (1983). Inversion of strong ground motion and teleseismic waveform data for the fault rupture history of the 1979 Imperial Valley, California, Earthquake, Bull. Seism. Soc. Am., 73, 6, 1553-1583, doi:10.1785/BSSA07306A1553.

Hartleb, R. D., J. F. Dolan, H. S. Akyüz and B. Yerli (2003). A 2000-year-long paleoseismologic record of earthquakes along the central North Anatolian Fault, from trenches at Alayurt, Turkey, Bull. Seism. Soc. Am., 93, 5, 1935-1954.

Hartzell, S. H., G. S. Stewart and C. Mendoza (1991). Comparison of L1 and L2 Norms in a teleseismic waveform inversion for the slip history of the Loma Prieta, California, earthquake, Bull. Seism. Soc. Am., 81, 1518-1539.

He, Z., Y. Zhang, W. Wang, Z. Wang et al. (2025). Revisiting the 2020 Mw 6.8 Elaziğ, Türkiye Earthquake with Physics-Based 3D Numerical Simulations Constrained by Geodetic and Seismic Observations, Remote Sens., 17, 720, doi:10.3390/rs17040720.

İmamoğlu, M. Ş. and E. Çetin (2007). Güneydoğu Anadolu Bölgesi ve Yakın Yöresinin Depremselliği. Dicle Üniversitesi, Ziya Gökalp Eğitim Fakültesi Dergisi, 9, 93-103.

Jackson, J., (1992), Partitioning of strike-slip and convergent motion between Eurasia and Arabia in Eastern Turkey and the Caucasus, J. Geophys. Res., 97, 12471-12479.

Jackson, J. and D. P. McKenzie (1984). Active tectonics of the Alpine-Himalayan belt between western Turkey and Pakistan, Geophys. J. Royal Astron. Soc., 77, 185-264, doi:10.1111/j.1365-246X.1984.tb01931.x.

Jeffreys, H. and K. E. Bullen (1958). Seismological Tables. Office of the British Association, Burlington House, London. 10.1038/151472e0.

Jolivet, L., C. Faccenna, B. Huet et al. (2013). Aegean tectonics: Strain localisation, slab tearing and trench retreat, Tectonophysics, 597, 1-33, doi:10.1016/j.tecto.2012.06.011.

Kahraman, M., D. G. Cornwell, D. A. Thompson, S. Rost et al. (2015). Crustal-scale shear zones and heterogeneous structure beneath the North Anatolian Fault Zone, Turkey, revealed by a high-density seismometer array, Earth and Planet. Sci. Lett., 430, 129-139, doi:10.1016/j.epsl.2015.08.014.

Kalafat, D., Y. Güneş. M. Kara, D. Pınar et al. (2007). Bütünleştirilmiş Homojen Türkiye Deprem Kataloğu (1900-2005; M ≥ 4.0): A revised and extended earthquake cataloque for Turkey since 1900 (M ≥ 4.0), Boğaziçi Üniversitesi Yayınları No: 977, 558s.

Karaoğlu, Ö., A. S. Selçuk and A. Gudmundson (2017). Tectonic controls on the Karlıova triple junction (Turkey): Implications for tectonic inversion and the initiation of volcanism, Tectonophysics, 694, 368-384, doi:10.1016/j.tecto.2016.11.018.

Karasözen, E., E. Nissen, P. Büyükakpınar, M.D. Cambaz et al. (2018). The 2017 July 20Mw 6.6 Bodrum-Kos earthquake illuminates active faulting in the Gulf of Gökova, SW Turkey, Geophys. J. Int., 214, 185-199, doi:10.1093/gji/ggy114.

Kenar, Ö. and M. N. Toksöz (1989). Anadolu yarımadasında yüzey dalgalarının dispersiyonu ve ortamın soğurma özellikleri, Jeofizik, 3, 92-106.

Ketin, İ (1977). A short explanation about the results of observations made in the region between Lake Van and Iranian border, Bull Geol Soc Turkey, 20, 79-85 (in Turkish).

Kikuchi, M., M. Nakamura and K. Yoshikawa (2003). Source rupture processes of the 1944 Tonankai earthquake and the 1945 Mikawa earthquake derived from low-gain seismograms, Earth Planets Space, 55, 159-172, doi:10.1186/BF03351745.

Kim, Y. S. and D. J. Sanderson (2006). Structural similarity and variety at the tips in a wide range of strike-slip faults: A review, Terra Nova, 18, 5, 330-344, doi:10.1111/j.1365-3121.2006.00697.x.

King, G. and J. Nabelek (1985). Role of fault bends in the initiation and termination of earthquake rupture, Science, 228, 984-987, doi:10.1126/science.228.4702.984.

Kiratzi, A., K. Papazachos, A. Özacar, A. Pinar et al. (2021). Characteristics of the 2020 Samos earthquake (Aegean Sea) using seismic data, Bull, Earthqu. Engin., doi:10.1007/s10518-021-01239-1.

Kirkpatrick, J. D., Z. K. Shipton, J. P. Evans et al. (2008). Strike-slip fault terminations at seismogenic depths: The structure and kinematics of the Glacier Lakes fault, Sierra Nevada United States, J. Geophys. Res.: Solid Earth, 113, B04304, doi:10.1029/2007 JB 005311.

Koçyiğit, A., A. Yılmaz, S. Adamia and S. Kuloshvili (2001). Neotectonics of East Anatolia plateau (Turkey) and lesser Caucasus: implication for transition from thrusting to strike-slip faulting, Geodinamica Acta, 14, 177-195.

Koketsu, K. (1985). The extended reflectivity method for synthetic nearfield seismograms, J. Phys. Earth, 33, 121-131, doi:10.4294/jpe1952.33.121.

Konca Özgun, A. S. Leprince, J.-P. Avouac and D. V. Helmberger (2010). Rupture Process of the 1999 Mw 7.1 Duzce Earthquake from Joint Analysis of SPOT, GPS, InSAR, Strong-Motion, and Teleseismic Data: A Supershear Rupture with Variable Rupture Velocity, Bull. Seism. Soc. Am., 100, 1, 267-288, doi:10.1785/0120090072.

Kozacı, Ö., J. F. Dolan, Ö. Yönlü and R. D. Hartleb (2011). Paleoseismologic evidence for the relatively regular recurrence of infrequent, large-magnitude earthquakes on the eastern North Anatolian fault at Yaylabeli, Turkey, Lithosphere, 3, 1, 37-54.

Lorenzo-Martín, F., F. Roth and R. Wang (2006). Elastic and inelastic triggering of earthquakes in the North Anatolian Fault zone, Tectonophysics, 424, 3-4, 271-289.

Mai, P. M., P. Spudich and J. Boatwright (2006). Hypocenter locations in finite-source rupture models, Bull. Seism. Soc. Am., 95, 965-980.

McClusky, S., S. Balassanian, A. Barka and C. Demir (2000). Global Positioning System constraints on plate kinematics and dynamics in the eastern Mediterranean and Caucasus, J. Geophys. Res., 105, B3, 5695-5719, doi:10.1029/1999JB900351.

McKenzie, D. P. (1972). Active tectonics of the Mediterrenean region, Geophys. J. Royal Astron. Soc., 30,109-185, doi:10.1111/j.1365-246X.1972.tb02351.x.

Mendoza, C. and S. Hartzell (1988), Inversion for slip distribution using teleseismic P waveforms: North Palm Springs, Borah Peak and Michoacan earthquakes. Bull. Seism. Soc. Am., 78, 1092-1111.

Muller, R. J., A. Aydın and F. Maerten (2003). Investigation of the transition between the 1967 Mudurnu Valley and 1999 izmit earthquakes along the North Anatolian Fault with static stress changes, Geophys. J. Int., 154, 471-482, doi:10.1046/j.1365-246X.2003.01968.x.

Nowroozi, A. A. (1972). Focal mechanisms of earthquakes in Persia, Turkey, west Pakistan, and Afghanistan and plate tectonics of the Middle East, Bull. Seism. Soc. Am., 62, 823-850, doi:10.1785/BSSA0620030823.

Nyst, M. and W. Thatcher (2004). New constraints on the active tectonic deformation of the Aegean, J. Geophys. Res., 109, B11406, doi:10.1029/2003JB002830.

Oglesby. D. D. and P. M. Mai (2012). Fault geometry, rupture dynamics and ground motion from potential earthquakes on the North Anatolian Fault under the Sea of Marmara, Geophys. J. Int., 188, 1071-1087, doi:10.1111/j.1365-246X.2011.05289.x.

Oppenheimer, D. H., W. H. Bakun and A. G. Lindh (1990). Slip partitioning of the Calveras Fault, California, and prospects for future earthquakes, J. Geophys. Res., 95, 8483-8498, doi:10.1029/JB095iB06p08483.

Özbakır, A. D., R. Govers and R. Wortel (2017). Active faults in the Anatolian-Aegean plate boundary region with Nubia. Turkish J. Earth Sci., 26, 1, 30-56, doi:10.3906/yer-1603-4.

Palyvos, N., D. Pantosti, C. Zabci and G. D'Addezio (2007). ''Paleoseismological evidence of recent earthquakes on the 1967 Mudurnu valley earthquake segment of the North Anatolian Fault zone'', Bull. Seism. Soc. Am., 97, 5, 1646-1661.

Pantosti, D., S. Pucci, N. Palyvos, P. M. De Martini et al. (2008), Paleoearthquakes of the Düzce fault (North Anatolian Fault Zone): Insights for large surface faulting earthquake recurrence, J. Geophys. Res., 113, B01309, doi:10.1029/2006JB004679.

Perinçek, D., Y. Günay and H. Kozlu (1987). New observations on strike-slip faults in east and southeast Anatolia. 7th Biannual Petroleum Congress of Turkey 89-103.

Pınar, A. (1995). Rupture process and spectra of some major Turkish earthquakes and their seismotectonic implications. PhD Thesis, Boğaziçi University.

Pınar, A., Y. Honkura and M. Kikuchi (1996). A rupture model for the 1967 Mudurnu Valley, Turkey earthquake and its implication for seismotectonics in the western part of the north Anatolian Fault Zone, Geophys. Res. Lett., 23, 1, 29-32, doi:10.1029/95GL03667.

Pondard, N., R. Armijo, G. C. P. King, B. Meyer and F. Flerit (2007). Fault interactions in the Sea of Marmara pull-apart (North AnatolianFault): earthquake clustering and propagating earthquake sequences, Geophys. J. Int., doi:10.1111/j.1365-246X.2007.03580.x.

Pucci, S., P. M. De Martini and D. Pantosti (2008). Preliminary slip rate estimates for the Düzce segment of the North Anatolian Fault Zone from offset geomorphic markers, Geomorph., 97, 538-554, doi:10.1016/j.geomorph. 2007.09.002.

Reilinger, R., S. McClusky, P. Vernant and S. Lawrence (2006). GPS constraints on continental deformation in the Africa-Arabia-Eurasia continental collision zone and implications for the dynamics of plate interactions, J. Geophys. Res. 111, B05411, doi:10.1029/2005JB004051.

Sançar, T., C. Zabcı, H. S. Akyüz et al. (2015). Distributed transpressive continental deformation: The Varto Fault Zone, eastern Turkey, Tectonophysics, 661, 99-111, doi:10.1016/j.tecto.2015.08.018.

Seyitoğlu, G., K. Esat and B. Kaypak (2017). The neotectonics of southeast Turkey, northern Syria, and Iraq: the internal structure of the Southeast Anatolian Wedge and its relationship with recent earthquakes, Turkish J. Earth Sci., 26, 2, 105-126, doi:10.3906/yer-1605-21.

Seymen, İ. and A. Aydın (1972). Bingöl deprem fayı ve bunun Kuzey Anadolu Fay Zonu ile ilişkisi, MTA Enstitüsü Bülteni 79, 1-8.

Shaw, B. and J. Jackson (2010). Earthquake mechanisms and active tectonics of the Hellenic subduction zone, Geophys. J. Int., 181, 2, 966-984. doi:10.1111/j.1365-246X.2010.04551.x.

Sibson, R. H. (1985). Stopping of earthquake ruptures at dilational fault jogs, Nature, 316, 248-251, doi:10.1038/316248a0.

Sieh, K. E. (1978). Slip along the San Andreas fault associated with the great 1857 earthquake, Bull. Seismol. Soc. Am., 68, 5, 1421-1448. doi:10.1785/BSSA0680051421.

Sieh, K. (1996). The repetition of large-earthquake ruptures, Proclamation of National Academy of Science, 93, 3764-3771.

Sibson, R. H. (1987). Earthquake rupturing as a mineralizing agent in hydrothermal systems, Geology, 15, 701-704, doi:10.1130/0091-7613(1987)15<701:ERAAMA>2.0.CO;2.

Somerville, P. G., N. F. Smith, R. W. Graves and N. Abrahamson (1997). Modification of empirical strong-ground motion attenuation relations to include the amplitude and duration effects of rupture directivity, Seism. Res. Lett. 68, 199-222, doi:10.1785/gssrl.68.1.199.

Stein, R. S., A. A. Barka and J. H. Dieterich (1997). Progressive failure of North Anatolian fault since 1939 by earthquake stress triggering, Geophys. J. Int., 128:594-604, doi:10.1111/j.1365-246X.1997.tb05321.x.

Stewart, G. S. and H. Kanamori (1982) Complexity of rupture in large strike slip earthquakes in Turkey, Phys. Earth Planet. Int., 28, 70-84, doi:10.1016/0031-9201(82)90118-2.

Şaroğlu, F., O. Emre and I. Kuscu (1992). Active fault map of Turkey. General Directorate of Mineral Research and Exploration, Ankara.

Şengör, A. M. C., O. Tüysüz, C. Imren et al. (2005). The North Anatolian Fault: A new look, Annu. Rev. Earth Planet. Sci. 33, 37-112, doi:10.1146/annurev.earth.32.101802.120415.

Tan, O., C. Tapırdamaz and A. Yörük (2008). The Earthquake Catalogues for Turkey, Turkish J. Earth Sci., 17, 405-418.

Taymaz, T., J. Jackson and D. McKenzie (1991a). Active tectonics of the north and central Aegean Sea. Geophysical Journal International 106(2):433-490. doi:10.1111/j.1365-246X.1991.tb03906.x.

Taymaz, T., H. Eyidoğan and J. Jackson (1991b). Source parameters of large earthquakes in the East Anatolian fault zone (Turkey), Geophys. J. Int., 106, 537-550, doi:10.1111/j.1365-246X.1991.tb06328.x.

Toksöz, M. N., J. Nabelek and E. Arpat (1978). Source properties of the 1976 earthquake in eastern Turkey: a comparison of field data and teleseismic results, Tectonophysics, 49, 199-205.

Utkucu, M. (2013). 23 October 2011 Van, Eastern Anatolia, earthquake (M_W 7.1) and seismotectonics of Lake Van Area, J. Seismol., 17, 783-805, doi:10.1007/s10950-012-9354-z.

Uzsoy, S. Z. and U. Ersoy (1969). Damage to reinforced concrete buildings caused by the July 22, 1967 earthquake in Turkey, Bull. Seismol. Soc. Am., 59, 2, 631-650, doi:10.1785/BSSA0590020631.

Vernant, P. (2015). What can we learn from 20 years of interseismic GPS measurements across strike-slip faults? Tectonophysics, 644-645, 22-39, doi:10.1016/j.tecto.2015.01.013.

Utkucu, M., S. Nalbant, J. McClusky et al. (2003). Slip distribution and stress changes associated with the 1999 November 12, Düzce (Turkey) earthquake ($M_w = 7.1$), Geophys. J. Int., 153, 229-241, doi:10.1046/j.1365-246X.2003.01904.x.

Wald, D. J., D. V. Helmberger and T. H. Heaton (1991). Rupture model of the 1989 Loma Prieta earthquake from the inversion of strong-motion and broadband teleseismic data, Bull. Seism. Soc. Am. 81, 5, 1540-1572, doi:10.1785/BSSA0810051540.

Wald, D. J. and T. H. Heaton (1994). Spatial and temporal distribution of slip for the 1992 Landers, California, earthquake, Bull. Seism. Soc. Am., 84, 668-691.

Wallace, R. E. (1968). Earthquake of August 19, 1966, Varto area eastern, Turkey, Bull. Seism. Soc. Am., 58, 1, 11-45, doi:10.1785/BSSA0580010011.

Walters, R. J., B. Parsons and T. J. Wright (2014). Constraining crustal velocity fields with InSAR for Eastern Turkey: Limits to the block-like behavior of Eastern Anatolia, J. Geophys, Res.: Solid Earth, 119, 6, 5215-5234, doi:10.1002/2013JB010909.

Wang, Z., W. Zhang, T. Taymaz, Z. He, T. Xu and Z. Zhang (2023). Dynamic rupture process of the 2023 *Mw* 7.8 Kahramanmaraş earthquake (SE Türkiye): Variable rupture speed and implications for seismic hazard, Geophys. Res. Lett., 50, e2023GL104787, doi:10.1029/2023GL104787.

Wessel, P. and W. H. Smith (1998). New, improved version of Generic Mapping Tools released, Eos, Trans. Am. Geophys. U., 79, 47, 579-579, doi:10.1029/98EO00426.

Wdowinski, S., Z. Ben-Avraham, R. Arvidsson and G. Ekström (2006). Seismotectonics of the Cyprian arc, Geophys. J. Int., 164, 1, 176-181, doi:10.1111/j.1365-246X.2005.02737.x.

Yagi, Y., M. Kikuchi, S. Yoshida and T. Sagiya (1999). Comparison of the coseismic rupture with the aftershock distribution in the Hyuga-Nada Earthquakes of 1996, Geophys. Res. Lett., 26, 20, 3161-3164, doi:10.1029/1999GL005340.

Yoshida, S. (1995). Waveform inversion methods for the earthquake source, J. Phys. Earth, 43, 183-209, doi:10.4294/jpe1952.43.183.

Zor, E., S. Özalaybey and C. Gürbüz (2006). The crustal structure of the eastern Marmara region, Turkey by teleseismic receiver functions, Geophys. J. Int., 167, 213-222, doi:10.1111/j.1365-246X.2006.03042.x.

Zor, E., E. Sandvol, C. Gürbüz, N. Turkelli et al. (2003). The crustal structure of the East Anatolian plateau (Turkey) from receiver functions, Geophys. Res. Lett., 30, 24, 8044, doi:10.1029/2003GL018192.

***CORRESPONDING AUTHOR: Hatice DURMUŞ**,
Kütahya Dumlupınar University, Engineering Faculty, Department of Geological Engineering, Kütahya, Türkiye
e-mail: hatice.durmus@dpu.edu.tr